A Study of the Detection of Defects in Ceramic Insulators Based on Radio Frequency Signatures.

by

Shaharyar Anjum

A thesis
presented to the University of Waterloo
in fulfillment of the
thesis requirement for the degree of
Master of Applied Science
in
Electrical and Computer Engineering

Waterloo, Ontario, Canada, 2014

I hearby declare that I am the sole author of this thesis. This is a true copy of the thesis, including any required final revisions as accepted by my examiners.

I understand that my thesis may be made electronically available to the public.

Abstract

The presence of defects in outdoor insulators ultimately results in the initiation of partial discharge (PD) activity. Because insulation failure and the consequent breakdown of power equipment can occur due to the cumulative adverse effects of partial discharges, it is important to detect PD activity in its early stages. Current techniques used in PD off-line analyses are not suitable for detecting defective insulators in the field. The work presented in this thesis involved the investigation of a number of cases of insulator defects, with the goal of developing an online RF-based PD technique for monitoring ceramic disc insulators that exhibit a variety of defects. The first three classes examined were an intentionally cracked ceramic insulator disc; a disc with a hole through the cap, which creates internal discharges; and a completely broken insulator disc. The fourth class involved an external corona noise using a point-to-plane setup. The defective discs were considered individually and were also incorporated into strings of 2, 3, and 4 insulators as a means of capturing the radiated RF signatures under external high voltage AC power. The captured RF pulses were processed in order to extract statistical, spectral, and wavelet packet based features. Feature reduction and selection is carried out and classification results pertaining to each feature-set type were obtained. To classify the discharges arising from different types of defects, an artificial neural network (ANN) algorithm was applied to the extracted features, and recognition rates of more than 90% were reported for each class. In addition, the position of the defective insulator within the string was varied and high defect classification results exceeding 90% were reported regardless of the position.

Acknowledgements

I am deeply in debt to my supervisor, Dr. Sheshakamal Jayaram, without whose support and guidance the completion of this thesis would not have been possible.

I feel deep gratitude to Dr. Ayman El-Hag, who provided very useful feedback and thoughtful insights into the online condition monitoring of insulation systems. I would also like to acknowledge Dr. Mohamed Kamel for the guidance he provided regarding data mining methods and their application.

Many thanks are due to my friends at HVEL, including Mahdi Khanali, Mohammed Saleh Moonesan, and Mohana Krishnan, for the wonderful time we spent together. Special thanks are due to my great friend Mantosh Devgan, with whom I spent many sleepless nights in the lab and the office.

I cannot even begin to thank my ammi (mother) for all the support and affection I received from her. My studies would never have been possible without her selfless devotion to my education beginning when I was a toddler. I also send enormous thanks to my father for being a strong example of such a high level of scholarly achievement and to my sisters, Mahrukh and Aleena, for their deep love and support.

Dedication

Dedicated to my parents.

Table of Contents

List of Tables

List of Figures

Chapter 1

Introduction

For the past few decades, owing to deregulation and competition, utilities across North America have been forced to make drastic alterations in the way they conduct business. The days of liberal spending on new assets as a means of achieving higher levels of system performance are long past. The focus is now increasingly shifting toward maximizing the utilization of existing assets and minimizing the huge capital investments needed for the replacement of costly equipment. In addition to these changes, increased demand for reliability and superior performance with respect to power equipment has also become far more significant in recent years.

Ageing assets pose significant challenges for utilities. The primary goal for the utility is to utilize the full life of an asset, but ageing increases the probability that the likelihood of equipment failure will become unacceptable from both a financial and a performance perspective [1]. The average age of vital assets, such as circuit breakers, transformers, insulators, cables, and poles, owned by transmission and distribution utilities in Ontario is estimated to be more than 35 years. Nearly 150 million porcelain suspension insulators are calculated to be currently deployed in North America [2]. A signficantly high proportion of these are either approaching or have exceeded the life time for which they were designed. These ageing assets are thus of special interest to North American utilities [3].

Improved utilization of utility assets translates to reduced capital expenditure and increased returns on the asset base. To defer the spending of huge capital amounts, many utilities are therefore increasing the loading on their equipment. Such decisions mean that less outage time is available for the de-energized testing, inspection,

and maintenance work required for in-service assets. Because it enables power lines to remain live during testing, online condition monitoring of power equipment has therefore attracted enormous interest both from the industry and academia. In particular, utilities have exhibited increased interest in appropriate online inspection tools and methods that can be utilized for assessing the electrical and mechanical performance of porcelain insulators.

1.1 Role of Outdoor Insulators in Transmission and Distribution Systems

Transmission and distribution lines play a crucial role in the delivery of electric power to the end consumer. Since a large part of power generation takes place at significant distances from the eventual consumer, transmission lines must be employed to carry the power generated to its destination. Figure 1.1 shows a simplified view of the generation, transmission, and distribution of AC power.

The transmission of AC power can be facilitated either through overhead lines or through underground cables. Concerns about cost have led to the predominant employment of overhead lines in transmission systems, while the tendency is to use underground systems in distribution systems because overhead systems are judged aesthetically unappealing in urban landscapes. Overhead transmission generally entails three primary components: a conductor, a tower structure, and an insulator, as depicted in Figure 1.2. Insulators serve two important functions: first and foremost, they isolate the conductor electrically from the grounded tower structure, and second, they serve as mechanical support for the conductor. To successfully fulfill their functions, insulators must be designed not only to withstand any electrical stresses that may occur throughout their long lifespans but also to tolerate the mechanical forces applied by elements such as wind and the weight of the conductor. The two main types of insulators commonly used in the industry are:

- Ceramic Insulators which include porcelain and glass.
- Polymeric, or composite, insulators.

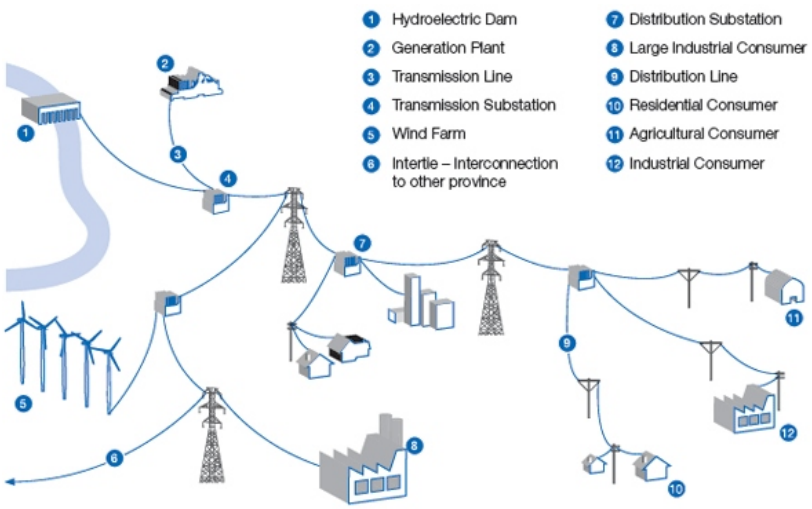

Figure 1.1: Simplified View of Generation, Transmission and Distribution [4].

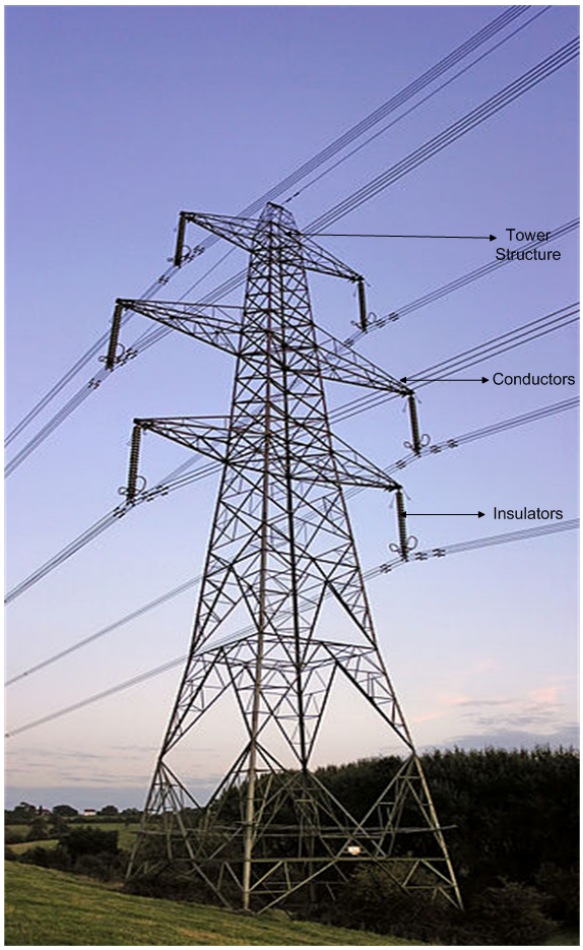

Figure 1.2: Transmission Tower Structure with Insulators and Conductors [5].

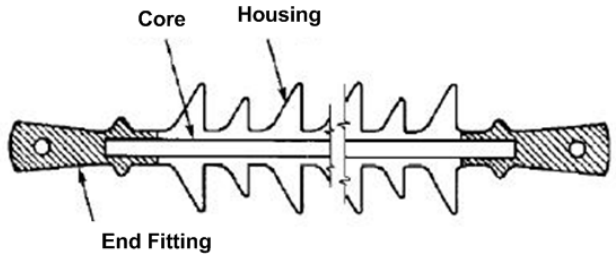

Figure 1.3: Polymeric Insulator Specimen [7].

1.1.1 Polymeric, or Composite, Insulators

Polymeric insulators, also called composite insulators , now represent a large share of the insulator market and are gaining acceptance from traditionally reluctant utilities due to the numerous advantages and appealing features they offer over porcelain and glass insulators: light weight, higher mechanical strength-to-weight ratio, superior performance under heavy contamination and wet conditions, and resistance to vandalism. Polymeric insulators account for 60% to 70% of newly deployed insulators [6]. Figure 1.3 illustrates a basic composite insulator.

The three major components of a polymeric insulator are the core, the housing, and the end fittings. The insulator must be strong enough to bear the substantial weight of the overhead conductors and should be designed to withstand such a mechanical load. To this end, the core is therefore constructed with fibre -reinforced plastic (FRP) as the dominant material. The end fittings, which are made primarily of forged steel, serve to join the ends of the insulator to the high-voltage line and the grounded tower. The final component, the housing, is composed primarily of silicone rubber, which enhances insulator performance by contributing properties such as hydrophobicity of the surface and protection of the core against moisture, sunlight, and corona discharge .

Despite the conspicuous advantages offered by polymeric insulators, they are still associated with the following disadvantages, which can justify support for the use of porcelain insulators, depending on the application:

- Polymeric surfaces are subject to chemical changes resulting from phenomena such as weathering and dry band arcing [8].

- Problems such as erosion and tracking can lead to complete failure of these insulators [9].
- Evaluating their life expectancy is difficult, and their long-term reliability is unknown.
- Detecting faulty insulators is challenging.

1.1.2 Porcelain Insulators

First introduced in 1909, porcelain insulators have been in use for well over a century and are well accepted by the industry: their application is most often considered a safe choice. Over the course of the century of their existence, many shell profiles and attachment hardware designs have been introduced; however, the design illustrated in Figure 1.4 is typical of a basic suspension-type porcelain insulator[10].

As can be seen in the figure, the key components of porcelain insulator design are the fired porcelain shell, which serves as the dielectric, and the hardware, which consists of an iron cap and a pin linked by Portland cement [7]. Although the dielectric breakdown strength of porcelain is a function of a range of parameters such as composition, temperature, and surface condition, the thickness of the specimen has the most profound effect, with an inversely exponential relationship between the dielectric breakdown strength and the specimen thickness. This effect occurs because increasing the thickness also elevates the chances of micro-defects being present within the bulk of the material. Indeed, the cracks and micro-voids that are introduced in the manufacturing stage have a severe effect on the puncture strength of the insulator. The primary purpose of attaching metallic hardware to the porcelain shell is to enable the materials to withstand the mechanical loading of the conductors. Failure of the metallic hardware can lead to the dropping of the overhead conductor. To prevent conductors from dropping and to ensure long life under service conditions that include corrosion and conductor galloping, high-quality metallic hardware free from cracks or defects is absolutely essential.

A third key element is the Portland type-1 cement that is used for joining the porcelain to the metallic hardware. Events such as lightning striking the transmission line can lead to the establishment of puncture paths inside the insulators. These paths

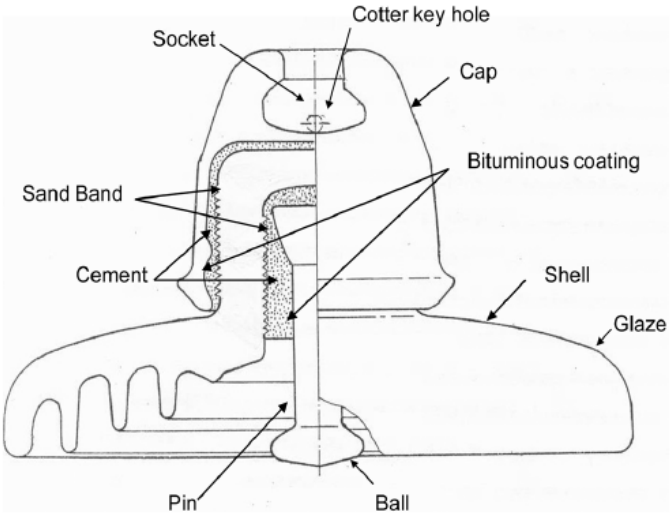

Figure 1.4: Typical Cap and Pin Type Porcelain Insulator Design. [7]

usually appear inside the cap where the cement glues the cap and pin to the porcelain [11].

Insulators are joined in series to form a string, which can be either a single string or multiple strings in parallel, depending on the application. The mechanical strength requirements are determined based on the number of parallel strings used whereas the electrical insulation requirements are established according to the individual insulators.

1.2 Ageing of porcelain Insulators

An understanding of the ageing mechanisms that occur in porcelain insulators is very important. These processes are described in specific detail in [12], a brief review of which is presented in this section.

1.2.1 Expansion of Cement

The expansion of Portland cement is a function of the growth characteristic associated with the composition of the cement and can lead to the formation of radial cracks within the insulators. Wet conditions can accelerate this expansion process due to the moisture absorbed by the cement. To quantify the amount of expansion that is needed to cause failure, Cherney and Hoton [13] conducted extensive water expansion

Figure 1.5: Hardware Corrosion [12].

tests on cement pastes as well as autoclave tests on insulators assembled with two different types of cement. They proposed an autoclave expansion limit of about 0.12% for suspension insulator grout, which was adopted as a guideline in ANSI C29.2.

1.2.2 Hardware corrosion

Improper electric stress grading can lead to corona discharge from the cap of the insulator in the area closer to the line end of the string. Such a corona can lead to the gradual removal of the galvanizing layer and the consequent exposure of the metallic cap to corrosion. The salt solution that results from high contamination levels and wet atmospheric conditions can cause leakage currents to flow across the insulator surface. This electrolytic action can create pin corrosion, which can cause loss of cross-section and mechanical strength in the pin. In the worst-case scenario, this type of damage could lead to the dropping of the conductor [11]. Such a highly corroded specimen is shown in Figure 1.5.

1.2.3 Mechanical and Electrical Stresses

During the course of the century in which porcelain insulators have been in use, manufacturing methods have improved dramatically. For this reason, significant variations

can be observed in the ageing characteristics of insulators belonging to different eras [14]. The manufacturing process involves cooling the porcelain from very high temperatures [11]. This procedure might introduce microcracks or very small defects, referred to as Griffith flaws, which occur because of differences in the thermal expansion coefficients of the raw materials. Such fractures may spread slowly if they are subjected to high concentrations of stress. The spreading might extend even further, to the point at which the insulator is no longer able to support the full voltage, even though it might still be able to support the conductor mechanically. This slow growth has the potential to cause irreversible damage to the insulator. In fact, the damage limit of the insulator is defined as the load at which this type of damage occurs. However, the insulator selection process used in North America is based on (1.1) and does not directly take into account this damage limit.

$$\frac{MechanicalandElectricalratedstrength}{MaximumServiceLoad} \geq 2.0 \tag{1.1}$$

where the ME rated strength is defined according to ANSIC29.2 and the maximum service load is defined according to ANSI C2 NESC .

Electrical insulators are designed so that flashover occurs without dielectric puncture when the insulator is subjected to electrical stresses greater than those for which it is designed. These high stresses could be a result of lightning or switching events which can have rise times as high as one million volts per microsecond. Such high stress levels can cause dielectric puncture [15]. Regularly occurring events like these can lead to partial breakdown of the porcelain which, over the long term, could create cracks along the circumference of the insulator. The disc may even eventually break o completely from the hardware, an event referred to as a donut failure.

1.2.4 Drying out of the bituminous coating

One improvement that has been incorporated into the design and manufacture of porcelain cap and pin insulators is the introduction of a bituminous layer that is applied to the cap and pin before the end fittings are joined to the dielectric with cement. The primary purpose of this layer is to cushion the forces created by hot and cold climate conditions so that mechanical stress risers are prevented. The bituminous

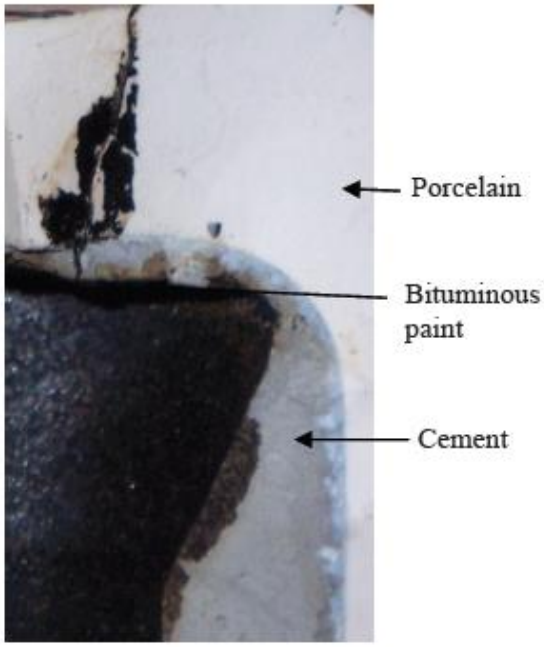

Figure 1.6: Bituminous Coating wear off [17].

layer also inhibits electrolytic action between the metallic surfaces and the alkalies in the cement. Over time, this layer loses resilience, which creates an uneven stress distribution in the porcelain that can cause cracking in the dielectric [16]. Poor quality of the interface between the bituminous coating and the cement can even lead to a puncture path, as shown in Figure 1.6.

1.3 Testing and evaluation of porcelain Insulators

Although only 5% of the direct capital spending on a power line is associated with insulators, 70% of line outages are attributable to deficiencies in their operation, and they represent nearly 50% of line maintenance costs [18]. Ageing of the insulators can have wide range of consequences; some can be detected visually but others require testing before they can be satisfactorily categorized. Some of the most commonly observed types of degradation include cracks of different shapes and dimensions, punctures, and broken discs. The traditional practice is to remove randomly selected insulator samples for degradation testing in a laboratory [19]. ANSI C29.2 specifies the design, quality conformance, and routine tests required for evaluating porcelain insulators.

1.4 Design Tests

Design tests are required to be carried out on every new insulator design. Some of the most important design tests are described in the following subsections.

1.4.1 Thermal-mechanical load cycle test

Thermal-mechanical load cycle testing is conducted in order to ascertain whether a specific design can withstand the combined effects of thermal and mechanical load cycles. The test requirements specify that 10 insulators be randomly selected to undergo extreme temperatures of -22°F (-30°C) and 104°F (40°C) for four 24 h cycles, with the heating period following the cooling period. At the same time, the insulators are also subjected to rated combined electrical and mechanical loading of 60%, as illustrated in Figure 1.7.The setup for tensile load testing is shown in Figure 1.8. Following the application of these four thermal load cycles, the insulators are cooled down to room temperature and then subjected to combined ME tests, as described in section 5.2 of ANSI C29.1.

Experience has shown that acceptance under these strict criteria is a strong indicator of good performance under harsh thermal and mechanical conditions.

1.4.2 Low-Frequency Flashover Tests under Dry and Wet Conditions

According to section 4.2 of ANSI C29.1, three insulators must be randomly selected for testing under both dry and wet conditions. For the dry condition testing, if the average flashover value fails to equal or exceed 95% of the rated flashover value, that batch of insulators is considered to have failed to meet the requirements of the standard. For wet conditions, the critical percentage is 90% of the rated flashover value.

1.4.3 Quality Conformance Tests

A number of quality conformance tests are also stipulated in ANSI C29.2. Manufactured insulators are tested for porosity, galvanization, dimensions, puncture resistance , and combined mechanical and electrical strength. To establish adherence to visual

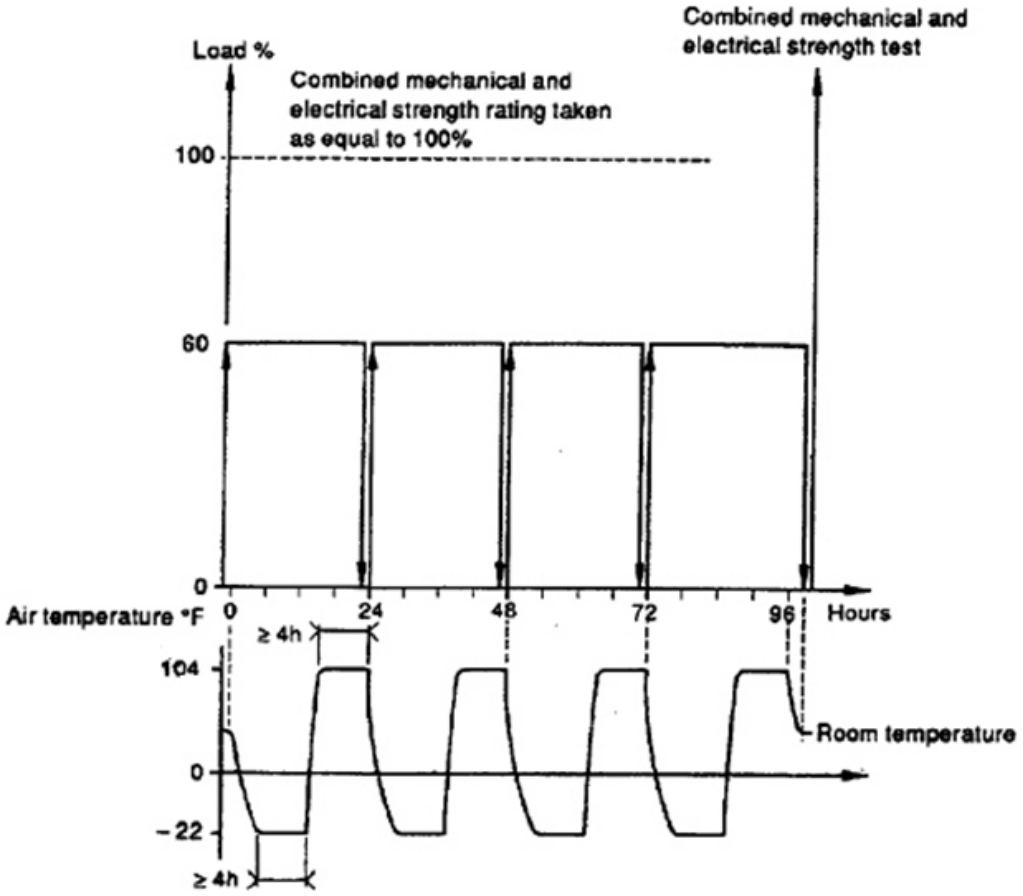

Figure 1.7: Thermal Mechanical Load Cycle Test.

Figure 1.8: Tensile Test setup[14]

Table 1.1: Maximum loads in kN (taken from ANSI C29.1).

ANSI Class 52-1	ANSI Class 52-2	ANSI Class 52-9A	ANSI Class 52-9B
5000	7500	5000	5000

and dimensional test requirements, three random samples are selected and checked against the manufacturers drawings. Failure of even one of these samples to conform to the manufacture-supplied values within the given tolerances means that the lot is considered to have failed to satisfy the standards requirements. For the porosity test, samples that were destroyed in previous destructive tests are soaked in dye, and its penetration into the dielectric is measured in order to determine whether that lot fails to meet the standard.

1.4.4 Routine Tests

Routine tests are included in the routine testing schedules of the utilities. The standards for these tests are also defined in ANSI C29.1. For porcelain insulators, the testing includes tension proof tests and flashover tests, the procedures for which are defined in ANSI C29.1. The tension proof test involves subjecting the insulator to the loads (in kN) listed in Table1.1. Insulators that do not meet the standards requirements are considered to have failed.

1.5 Online Condition Monitoring of Insulators

The enormous demand for reliable power delivery has created pressure for utilities to keep transmission lines in operation as much as possible without disruptions. Achieving this goal requires maintenance work, which might entail interrupting the flow of power in the lines. Online condition monitoring of the lines has therefore become very important because it does not require the lines to be de-energised before work can commence, and the personnel who perform maintenance work or routine tests on the lines can perform the required tasks on live lines . To maintain their safety under these conditions, when conducting field tests on insulators, the line men must first determine the number of defective units in a string of insulators so that they can ensure that the remainder of the string is comprised of units that are capable

Table 1.2: Typical Number of Porcelain Insulators for different Voltage Levels

Nominal System Voltage(kV)	Maximum Nominal System Voltage	Typical Number of Units
115	121	7-9
138	145	7-10
161	169	9-14
230	242	11-16
345	362	16-18
500	550	24-26
765	800	30-37

of providing adequate insulation that will protect them while they work. Evaluating the insulating ability of a string of insulators is dependent on the following conditions [20]:

- The number of defective units in the string.
- The position of the defective units within the string.
- The position of the line worker.

For a variety of line ratings, Table1.2 shows the typical corresponding number of insulator units in a line.

1.5.1 Minimum Number of Healthy Insulators for Live line work

The transient overvoltages that occur as a result of switching operations induce the most severe voltage stresses. A key safety requirement is that live line workers not be closer than a minimum approach distance calculated for the highest overvoltage transient that is anticipated in the workspace [2].]. As pointed out earlier having defective units would reduce the ability of the insulators to protect the live line workers from any switching overvoltages that may arise. For this reason, the minimum number of healthy insulators must be calculated for each of the strings. The method discussed here is based on the CIGRE formula (1.2), as follows [20]:

$$U_{\mathrm{b}} = U_{\mathrm{o}}(1 - 0.8[\frac{N_{\mathrm{b}}}{N_{\mathrm{o}}}]k) \tag{1.2}$$

where,

U_b: Transient overvoltage with a 50% probability of sparkover for a string of insulators that includes faulty units

U_o: Transient overvoltage with a 50% probability of sparkover for a string of insulators in which all units are healthy

N_b: Number of defective units in the string

N_0: Total number of units in the string

k: Empirical coefficient that characterizes the average dielectric strength of the defective units

The CIGRE formula is quite conservative and assumes that defective insulators are placed in the worst possible location within the string. This formula was used for calculating the values listed in Table 1.3, which shows the minimum number of healthy units $N_g = N_o - N_b$ for a range of system voltages and for a variety of values that indicate the maximum overvoltage transients (expressed per unit of the system voltage).

1.6 Online Condition Monitoring Techniques

This section describes condition monitoring techniques used for the detection and diagnosis of porcelain insulator defects. Some techniques, such as visual inspection and hi-pot testing, are well-accepted methods with standards that provide guidelines for their application. The use of other methods, such as infrared scanning, is accompanied by reservations, and they are not widely employed.

1.6.1 Visual inspection

This method provides a simple and cost-effective means of detecting specific obvious defects such as heavy corrosion of the metal hardware, broken shells, and large cracks. The success of this technique is largely dependent on the level of detail that can be perceived from the observation point. Very high-powered binoculars mounted on a

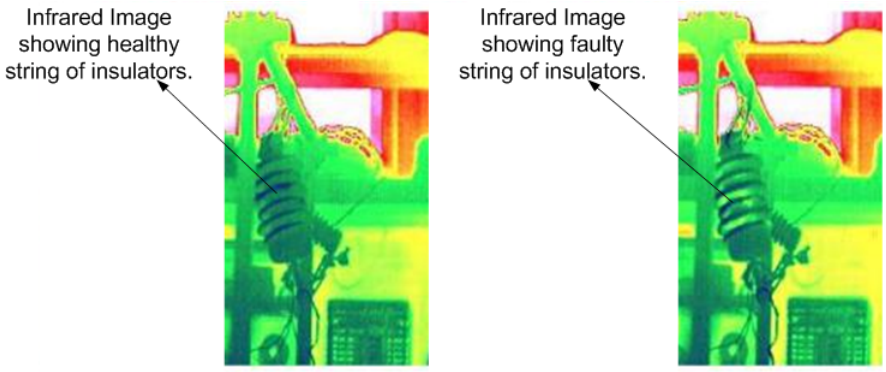

Figure 1.9: Infrared Images of the insulators (Left) Healthy Insulator String (Right) Faulty Insulator [22].

stable viewing point should be employed for these observations. Of course, not every defect can be detected in this way, either due to the low level of detail resolution or simply because the insulator is in a visually inaccessible location. This method is therefore employed only as part of a routine line patrol, and more reliable methods must be used in conjunction with it in order to provide more thorough inspections [21].

1.6.2 Infrared Scanning

A useful, albeit not completely fail-safe, inspection tool is infrared, or thermal, imaging of the insulators. It can be employed for detecting a number of problems that influence the performance of porcelain insulators. However, it also entails several limitations that negatively affect its application. Field conditions have very precise requirements: there should be no wind or solar flux, etc. The temperature rise that indicates different defect conditions has a very narrow range: 10 °F to 8°F . In addition, the heating effect can typically be detected only beneath the porcelain bell and the insulators that are nearest to the high-voltage end of the line [19].The potential for an automatic fault detection system was shown in [22] based on thermal imaging technique. Figure 1.9 provides a comparison of thermal images that the authors of the study obtained for both a healthy and a faulty string of insulators.

Figure 1.10: Hi-Pot Field Test.

1.6.3 Hi-Pot Test

A well-established method used by utilities worldwide for testing porcelain insulators, the hi-pot test offers a high degree of accuracy with respect to the detection of faulty insulators. With this test, the line men must physically test each disc in the string for punctures. When the tester is pressed against the insulator string for 10 sec, any ow of leakage current that exceeds the normal capacitive leakage current value causes the tester to emit a beeping sound, indicating a faulty unit [23]. The main drawback of this method is the requirement for physical contact with the insulator hardware and the consequent close proximity of the line worker. Figure 1.10 illustrates a line worker carrying out the Hi-pot test on a 115kV line.

1.6.4 Electric Field Mapping

The distribution of electric elds along the insulator string is measured using a variety of electric field probes. The images obtained are compared with those of a defect-free string, enabling the identification of faulty insulators [24; 25].

1.6.5 Ultrasound Based Detection Techniques

Ultrasound diagnostic methods are based on the principles of pulse echo or acoustic emission detection. The acoustic waves that propagate through a material are affected by the presence of flaws such as voids and cracks, and signature changes occur in their velocity, direction, and attenuation. Sensors are used for detecting these changes in the acoustic reflections, and the nature of the defects can be established based on the characteristic reflections of the acoustic waves produced by the electrical discharges that accompany the presence of defects [26].

1.7 Thesis Organisation

An outline of the the thesis is as follows:

- Chapter 1 reviews the dominant outdoor insulator technologies along with their role within the power transmission network. Further, the ageing mechanisms of porcelain insulators along with their their testing methods are reviewed. Finally a brief overview of some of the condition monitoring methods for ceramic insulators is presented.

- Chapter 2 reviews the most important research literature associated with RF based condition monitoring techniques for power equipment like Gas insulated switchgear and Transformers. Preliminary research work associated with the burgeoning field of RF based condition monitoring for outdoor insulators is also presented and the gaps in the state of the art are identified.

- Chapter 3 outlines the details of the porcelain insulator samples that are used in the experimental work. The details of the data acquisition technique for the PD RF signatures is outlined. A broad description of the experiments that are a part of this study is presented. The experimental test setup used for the data acquisition in each of these experiments is elaborated The selection and sensitivity analyses of the RF antenna are also a part of this chapter.

- Chapter 4 presents the details of the classification tools (algorithms) that are used to classify the classes of defects are also a laid out. The wavelet packet

decomposition technique which is also used as a feature extraction technique is described. In addition the feature extraction techniques and the extracted features are also discussed.

- The extracted features are used to train and test the classifier ANN as described in Chapter 4. In Chapter 5 the classification performance results are presented for the single disc and the string of insulators using statistical, FFT and WPD based features. In addition the classification performance corresponding to variation of the defect location within the string is presented.

- Chapter 6 presents the conclusion for the research work carried out in the thesis. In addition future work in the field of RF based condition monitoring of ceramic insulator is discussed in this chapter.

Table 1.3: Minimum Number of Good Insulators for live line work [20]

Maximum System Voltage	Maximum Anticipated Voltage Rise		3.0 pu Formula	Based on CIGRE
kVp-p/p-g	pu	kV p-g	Ng	Ng Porcelain
121/70	3.0	349	8	
	2.2	256		5
	2.0	233		4
	1.7	198		3
145/84	3.0	418	9	
	2.2	307		6
	2.0	279		5
	1.7	237		3
169/98	3.0	489	11	
	2.2	359		7
	2.0	326		5
	1.7	277		4
242/140	3.0	699	14	
	2.2	512		8
	2.0	466		7
	1.7	396		4
362/140	3.0	1043	17	
	2.2	765		10
	2.0	695		8
	1.7	591		5
550/317	2.0	1265	25	
	2.4	1106		22
	2..0	1054		19
	1.7	896		13
800/462	2.0	1536	32	
	1.9	1460		30
	1.7	1306		24

Chapter 2

Condition Monitoring of High Voltage Insulation based on Radio Frequency Techniques

2.1 Partial Discharge

Partial discharge (PD) refers to the incomplete breakdown of the insulation systems. The IEC 60270 standard defines PD as "the localized electrical discharge that only partially bridges the insulation between conductors and which can or cannot occur adjacent to the conductor"[27].

Partial discharge has been a known phenomenon since the start of the twentieth century when high voltage technology was in its nascent stages. Over the latter half of the last century the importance of PD measurement and analysis has been realized and its use as a non-destructive technique for testing power equipment enclosing various kinds of insulating systems has become established. Existence of PD within the insulation causes the inevitable accelerated aging of the insulation and eventual failure of these systems. PD results in the PD current pulses across the PD site due to the acceleration of the charge. The IEC 60270 standard lays out the requirements for traditional PD measurements which characterizes PD in terms of apparent charge. This conventional measurement of PD is based on capacitive decoupling and a detection unit.

2.1.1 Partial Discharge Measurement and Characterization

Different physical changes result as a consequence of the PD phenomenon and a number of PD measurement methods are based around the measurement of these changes[28]. For example the IEC 60270 standard which is the most widely adopted method by the industry centers around the characterization of PD currents. PD also results in the formation of a number of gases and Dissolved Gas Analysis is based on the accurate analysis of the various gaseous components. Similarly PD can cause acoustic emissions and the measurements of these acoustic waves comprise another PD measurement technique. As will be discussed in subsequent sections PD also results in electromagnetic radiation within the radio frequency (RF) band and PD measurement using RF techniques has received a lot of research attention in recent years. Depending upon the application area some of these methods have an inherent advantage over the other ones.

2.1.2 Radio Frequency (RF) Emissions as a Consequence of PD Activity

As a consequence of PD activity, the PD current at the discharge site has a rise time in the order of nanoseconds. The subsequent rapid acceleration of this charge means that spectra with frequencies well into the radio frequency region ranging from 200MHz and above are radiated into the free space surrounding the discharge site [29]. This electromagnetic radiation is directly related to the rate of change of the current. Wideband antennas can be used to detect and capture these electromagnetic radiations. It was shown by P J Moore et al that the wideband array of antennas can be employed to detect the location of the PD source using an iterative algorithm if the location of the PD source is within 15 m from the antenna array[30]. The primary enabler in such radiometric systems is the high speed digital sampling technology that is become available in the recent times[31] which allows direct sampling of the antenna data without being down converted prior to sampling. This translates to a high fidelity signal. The possible advantages include:

- No contact with the high voltage bus or high voltage line end.
- Non-invasive to the plant being monitored.

- Improved safety for the operators and testing personnel.

2.2 Radiometric PD detection in Gas Insulated Switchgear (GIS)

Gas insulated switchgear offer the advantages of being highly compact and require very less maintenance effort and are have therefore been widely adopted by the industry. Moreover, they are characterized by their high availability and reliability. For these requirements to be met on a continuous basis, PD measurements are performed at the time of factory quality assurance using IEC 270[32] standard and also for condition monitoring of the switchgear during the field application. The IEC 270 is always performed at the time of factory quality assurance tests, this method cannot be applied for online condition monitoring during field operation because it is a low frequency method and suffers from high interference from a variety of sources including electromagnetic interference and interference from other substation equipment. High frequency methods like the VHF (very high frequency) method have been applied to circumvent this problem with limited degree of success.

The corona induced interferences due to the incoming overhead lines have a larger magnitude compared to the PD induced in the switchgear. And corona in air is found to have spectra that falls roughly in the same range as VHF (100 - 300 MHz). This poses a great problem because it becomes extremely difficult to distinguish between the PD induced within the Switchgear and corona due to the incoming overhead lines.

This problem can be conveniently overcome by moving to an even higher frequency range, the ultra-high frequency (UHF) range in which PD is measured and detected in the 300MHz to 3GHz by using UHF sensors [33; 34; 35]
. This method makes use of the fact that the PD activity within the SF_6 gas results in radiation that goes into the UHF range [36]. However the corona in air does not have significant energy presence in this frequency region and by employing specially designed high pass filters any interfering corona signals can be effectively suppressed.

2.2.1 UHF Based PD Detection in GIS

UHF based PD detection has attracted a significant amount of research interest in recent years because it can be applied for online PD detection and measurement in GIS owing to its anti-interference properties. This is advantageous because it replaces the use of costly coupling capacitors with built in sensors within the station terminals of the GIS equipment. The major research literature is mainly focused towards the following:

- Issues related to the UHF sensor design, selection and its placement [37; 38; 39; 40]
- Measurement and detection characteristics of the antennas and the PD patterns resulting from various defects[41; 42; 43].
- Localization methods of the PD source using UHF measurements[44; 45].

2.2.2 UHF Sensor Design and its Placement

One of the main components in GIS radiometric PD detection is the sensor or the UHF antenna. There are two types of sensors, the inner sensor and the external sensor. The inner sensor offers the advantage of high detection sensitivity but it is difficult to install it on the GIS equipment in service, so it must be installed at the time of the manufacture and it may alter the field distribution within the GIS as well[46]. The external sensors are the preferred choice since they can be installed on the GIS equipment already in service and also because they do not influence the electrical field internal to the GIS. The external sensors are usually installed at the insulation spacer of the GIS tank [47].

Microstrip antenna technique has recently been developed and the development of a Rectangular Microstrip Patch Antenna (RMPA) was reported in [37] which was fixed at the spacer of the GIS. The RMPA sensor is designed for the measurement of the UHF signals from the GIS. Parameters like antenna substrate material, the thickness of the cavity and the coaxial line feed of impedance match are optimized for frequency band widening hence overcoming the problem of narrow bandwidth. The working bandwidth of the designed sensor was reported to be 340 to 440 MHz

with relative bandwidth of 25.6% . For interference suppression the sensor is packaged with an aerial cover and the authors claim it to have a better performance than inner loop and inner disc plate sensors.

The placement of the UHF sensor plays a crucial role in the measurement of PD within GIS. The placement of the sensor affects the final output signal and also the propagated electromagnetic wave because the signal gets attenuated in various directions and positions. The EM wave is able to travel long distances because of the similarity of the GIS structure to a coaxial waveguide but at the same time there are considerable number of reflections and refractions within the GIS owing to the presence of some complicated L section and T-branch structures. These considerations influence the propagation and attenuation of the EM wave. A number of recent research studies have been carried out related to the propagation characteristics of UHF EM wave in GIS but most of them have ignored the components in other directions in favor of the radial direction component [48; 49; 50].

Tianhui et al addressed this issue in [40] where they considered the propagation of the components in the axial as well as perpendicular directions to the GIS tank. As a first step they analysed the attenuation at different radial positions using the FDTD (finite difference time domain) technique. Subsequently they calculated the signal components in the other two directions. Having calculated the coupled signals in all three directions the signals received for different directions and circumferential angles were compared to obtain peak to peak value and cumulative energy of the voltage in each of the three cases. This allowed them to describe the attenuation characteristics due to the placement of the sensor based on which a new method for circumferential and axial location was proposed.

2.2.3 Antenna Detection Characteristics

The external antennas used for UHF measurement in GIS are designed to detect the radiation that leaks outside from inside the GIS. The antenna is installed on the insulation spacer which is fixe d teo the GIS tank through tightening bolts. The EM radiation is leaked out from the spacing beween the solid insulator and the bolts and the number of these bolts affect the leaked EM waves. There are different types of antennas available and have been used in the different research studies. Kaneko et

al compared different antennas for the frequency characteristics of various antennas and studied the effects of the position of the antenna and the number of bolts on the frequency response [41]. They also reported the dependence of maximum detected voltage on the distance of the antenna from the spacers for different types of antennas.

The specific defects within the GIS can result in different PD patterns and this has the potential to serve as the basis for distinguishing between the different defects. There are a variety of defects that could be present within the GIS such as a protrusion on high voltage conductor, floating electrode, free metal particle, and particle on the spacer, void and aerial and external defects. These defects were artificially created within a GIS in[42] and the corresponding PD patterns were obtained for each type of defect which included the peak to peak value and the transmission rate of the EM wave for each type of defect. Harmful metallic particles within the GIS affect the reliability of the insulation and they are difficult to detect using other means. The authors in [43] studied the influence of these particles on the PD signal that was detectable by the antenna. They studied three different locations of such particles ranging from particles placed on the center conductor, a particle adhering to the spacers surface and a free particle. They found that the PD signal generated by the free particle was stronger than the particle placed on the center conductor by one order of magnitude. The magnitude of PD signal generated due to a particle sticking to the spacers surface was in between the two values, depending upon where it was adhering to the spacer.

2.2.4 PD Localization in GIS based on UHF Measurements

The UHF techniques are applied in order to detect PD in GIS with considerable degree of accuracy and this method is also applied for localizing the PD source using methods like time of flight and the frequency domain method. The time of flight method relies on the emission of the very fast electric pulses with rise time below 1 ns. Locating PD source in GIS equipment is essentially a one dimensional problem. It utilizes two sensors located at a known distance X from each other with X_1 and X_2 being the distances between the PD source and the two sensors respectively as shown in Figure 2.1. The distance X_1 can then be calculated as given in [44].

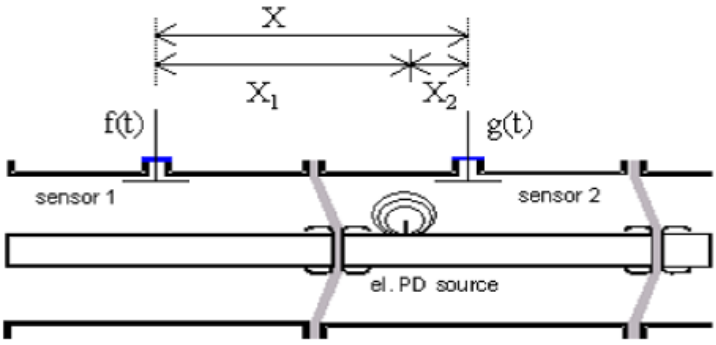

Figure 2.1: PD location in GIS using time of flight method.

2.3 Radiometric PD Detection in Transformers

Since the first UHF based PD monitoring system was installed for GISs in 1986 at Torness nuclear power station in Scotland, it has now become a commercially viable solution for online monitoring [51]. However, the UHF based PD monitoring for transformers, is still in its infancy [52] but its application to transformers can be swift because it can build upon the vast foundation of experience and knowledge gained from the application to GIS. Like GISs the placement of sensors is preferred to be external to the transformer thus affording the advantages of ease of removal and equipping in-service transformers with the UHF monitoring system. Furthermore similar to GIS the UHF technique applied to the transformers offers good immunity against corona induced interference.

In contrast to the GIS, the location of PD within the transformer tank is a 3 dimensional problem and hence more challenging than the latter. It requires at least 3 antennas and the calculation of three time differences (Δt_1, Δt_2, Δt_3) for the antennas using a procedure which is outlined in [23].

2.4 Radiometric PD Detection in Outdoor Insulators

The area of RF based condition monitoring of outdoor insulators is still quite nascent even though detection and localization of PD using RF measurements is now a matured discipline in gas insulated switchgear and transformers. However the applicability of this method to outdoor insulation has been demonstrated and is advantageous

for the same reasons as discussed for transformers and switchgears. In fact, the existence of distinctive radio noise broadband frequency components for the discharge activity taking place within the polymeric and porcelain insulator samples has been confirmed [53]. The encouraging aspect of these results was that distinctive broadband frequency components were clearly observed for different samples indicating that there is a relationship between the specific discharge phenomenon and the radiated energy.

Also, Ibrahim et al. presented results of an initial investigation into the use of RF sensing techniques for polymeric insulator specimens [54] along with the feasibility of classification of the partial discharges. These preliminary studies have used simple geometries for the test samples and the effect of actual insulator profiles on the PD has not been investigated. They considered 4 different PD sources resulting from the polymeric surface. The first source comprised of a water droplet resting on top of the polymeric surface followed by a PD due to a sharp edge at the grounded electrode, the third case was comprised of PD due to sharp edge at the high voltage electrode. Finally the combined effect of PD due to combination of sharp edge and water droplet comprised the last PD source. From these four PD sources the authors were able to extract FFT based features and only selected the features that had high recognition rates, discarding the rest of the features. With these features the authors reported an encouraging overall recognition rate of 93% using artificial neural networks.

The potential of a VHF (very high frequency; 30 - 300MHz) method to monitor the physical condition of porcelain insulators is reported by Wong using fractal analysis [55]. The author considered four different porcelain insulator specimens with the same type of defect being surface cracks. A fifth completely new insulator sample was also considered as a control sample for the study. Next the whole setup was energized and the VHF signals were acquired using a bi-conical antenna. A series of signal processing techniques were applied to this data in order for filtering out the unwanted components. The power spectral density plots of the signals showed most components in the 1-200 MHz range which complemented the micro second range in which the time domain signals existed. Not being able to have discriminatory features for the FFT results for different defects, the author used the fractal analysis method to distinguish between the four cases by plotting the fractal dimensions against each

specimen.

Further, a vehicle mounted system that is capable of detecting and locating the faulty string of insulators on a transmission line, based on the time delay between arrays of 4 antennas has been reported [56].

However, if the detection is based on using partial discharge (PD) activities as a means of the insulation degradation, in order to make the detection effective, it is required to use an ultra-high frequency (UHF; 300MHz 3GHz) range as detection limits. Also, in identifying different types of defects, classification of the PD activities is necessary.

2.5 Research Objectives

In this chapter, the RF-based PD detection technique applied to high-voltage insulation in a variety of insulation systems such as GIS, transformers, and outdoor insulation was reviewed. It can be concluded that the technique has been applied with a reasonable amount of success to GIS and transformers and that the various issues concerning its application are well understood. A significant amount of work has also been reported relative to locating the source of the PD in this equipment though a number of techniques such as the time-of-flight method and the frequency domain method. Further investigation related to PD patterns for a variety of defects has also been conducted. Very little work has been performed with respect to the application of these techniques for outdoor porcelain cap and pin insulators. Even fewer studies have examined the application of artificial intelligent algorithms or other algorithms for the classification of the data associated with different defect cases. With this background, the following were the objectives of this thesis:

- To conduct an experiment designed to provide an understanding of the effect of antenna placement on the electromagnetic emissions captured from defective porcelain insulator discs

- To carry out an experiment designed to acquire RF PD data that correspond to electromagnetic emissions due to defective single porcelain discs, to extract features from this data, and to classify the features to ensure the feasibility of

this technique for defect classification

- To use an ANN algorithm to complete a detailed study of the potential for defect classification in a string of up to four insulators, with the defective insulator always connected to the high-voltage end
- To investigate the effect of varying the location of the defective disc within the string on the PD signatures and on the feasibility of their successful classication

Chapter 3

Material and Methods

Until present, very few research studies have focused on RF based PD detection and classification on actual ceramic insulator samples taking their complete profile into consideration. This chapter outlines the details of the porcelain insulator samples that are used in the experimental work. The details of the data acquisition technique for the PD RF signatures is outlined. A broad description of the experiments that are a part of this study is presented. The experimental test setup used for the data acquisition in each of these experiments is elaborated The selection and sensitivity analyses of the RF antenna are also a part of this chapter.

3.1 Defects in Porcelain insulators

As explained in Chapter 1 the ceramic insulators are subjected to significant mechanical an electrical stresses throughout their operational lifetimes.The test samples in this study comprise of defective insulator shells of three different types. The defects in ceramic insulators can arise either during the manufacturing process itself as micro defects or introduced later on when they are in service due to high electrical stress.These defects can grow with age when under operation. The defects that are most frequently encountered by the utilities include cracked shells, broken shells, and completely punctured insulators.Some of the most commonly observed of these resulting defects are illustrated in Figure 3.1. All of these lead to the initiation of PD activity within the insulator and contribute to accelerated failure of the insulators.

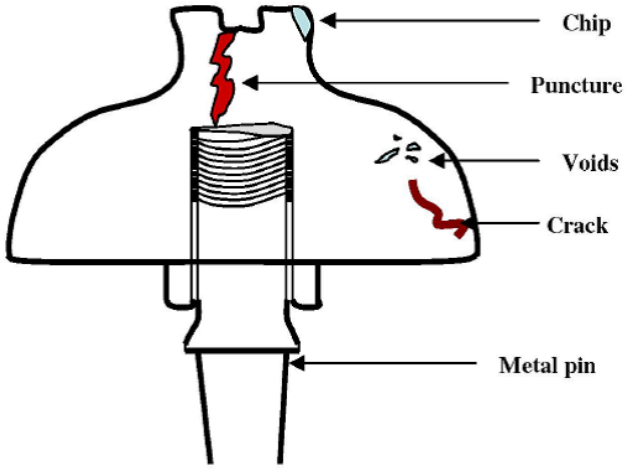

Figure 3.1: Different types of defects in a porcelain insulator disc. [21]

3.2 Porcelain Disc with a deliberately Introduced Crack

Figure 3.2 shows a ceramic insulator disc in which a crack was introduced deliberately to obtain the radiation patterns resulting from this type of defect. The radiated electromagnetic energy will be dependent on the shape, size and the length of the cavity hence changing these parameters would change the features of the radiated signatures. The crack in the insulator shell can be considered to be a cavity and this leads us to the classical capacitor model of an air filled cavity within a dielectric.

3.3 Broken Disc

Figure 3.3 shows a ceramic insulator disc with a significant portion broken off. This type of defect can be easily detected visually if the disc is incorporated in the visible part of the string. However the detection becomes a problem if the defective insulator is present in visually inaccessible region of the string. An insulator shell of similar rating was broken off in order to acquire the corresponding radiation patterns.

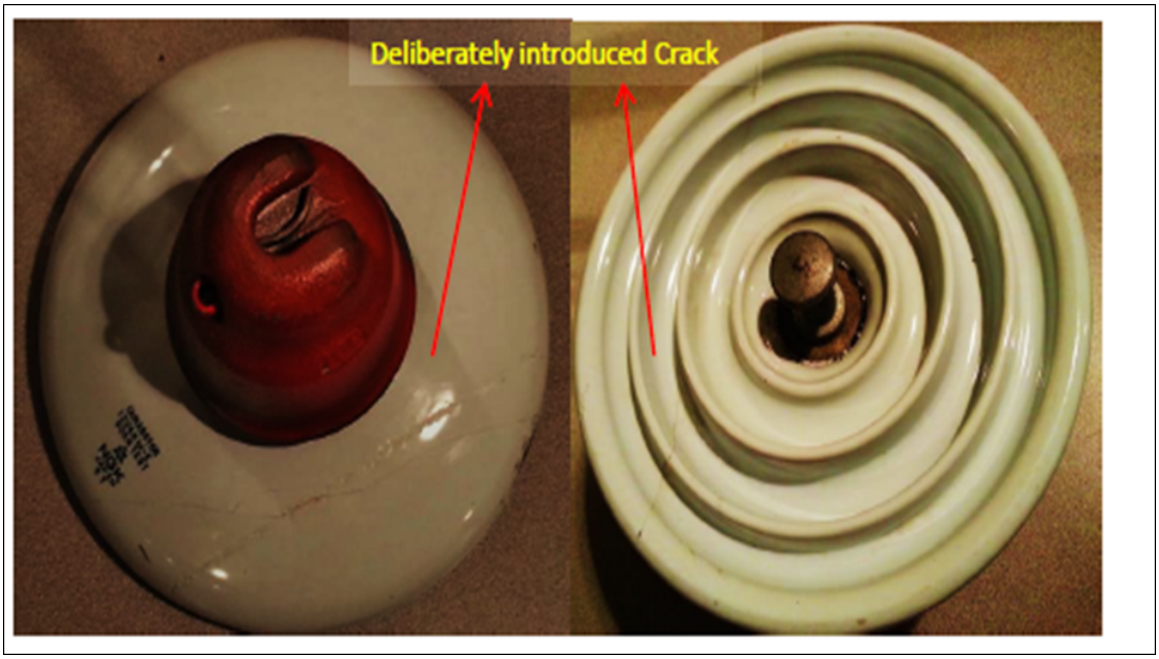

Figure 3.2: Porcelain Disc with a deliberately introduced crack.

Figure 3.3: Broken Disc.

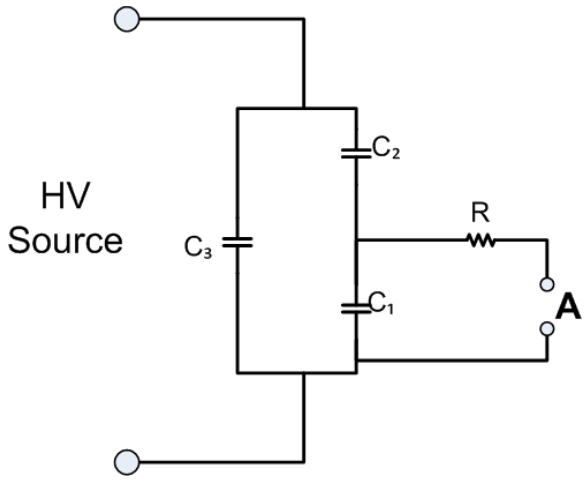

Figure 3.4: An equivalent circuit representation of a hole through the cap defect.

Figure 3.5: Insulator with a hole through the cap.

3.4 Hole Through the Cap

The third defect comprises of a hole through the cap of the insulator as shown in Figure 3.18. This hole would initiate internal discharges within the cap of the insulator and inclusion of this type of defect would allow us to examine the differences in RF signatures of three different PD mechanisms. C_1 can be considered to be the

capacitance of the hole or gaseous inclusion within the cap of the insulator. The dielectric surrounding the hole can be considered to be in series with the resulting capacitance of the healthy dielectric C_2. A comparatively large capacitance C_3 in parallel with the series arrangement of C_1 and C_2 represents the rest of the insulator sample. A spark gap A in parallel with the capacitance C1 models the breakdown of the hole at a sufficiently high potential across it experiencing a breakdown resistance R as shown in Figure 3.18.

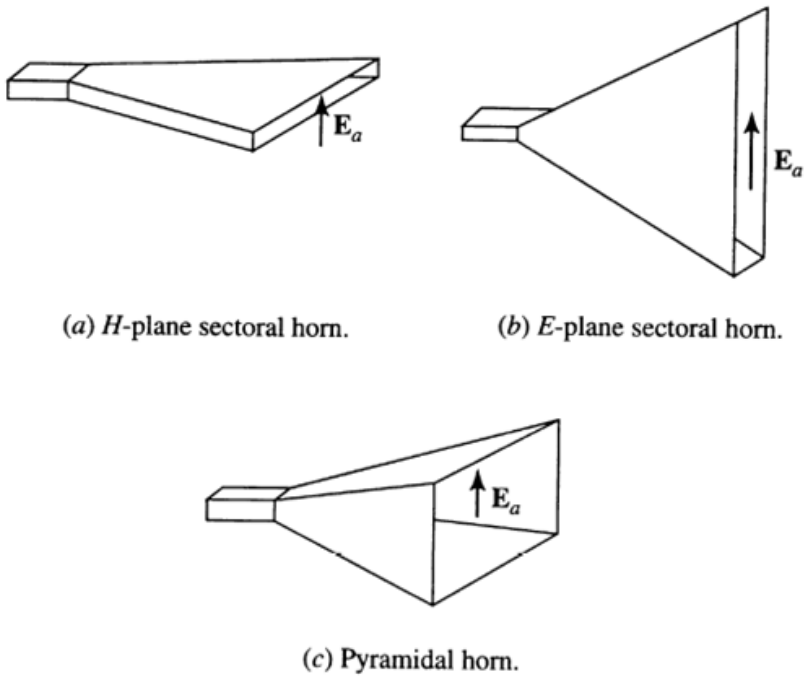

(*a*) *H*-plane sectoral horn. (*b*) *E*-plane sectoral horn.

(*c*) Pyramidal horn.

Figure 3.6: Different Constructions of Horn Antennas [57].

3.5 RF Antenna Selection

Horn antennas are widely used for measurements in the 300MHz − 3GHz (UHF) range. They offer advantages such as high bandwidth, high gain and low voltage standing wave ratios (VSWR)[1]. The construction of these antennas can differ based on the direction of the flaring. Based on this there are three types (a) the horn flared in the direction of Elevation plane (E-plane) only (b) the horn flared in the direction of Horizontal plane (H-plane) only (c) Pyramidal horn antenna which is flared in both

the E and the H plane. The flare is mostly linear; however, circular and exponential flare antennas are also used in certain applications. Figure 3.6 shows the simple construction of the E-plane, H-plane and the pyramid type horn antennas.

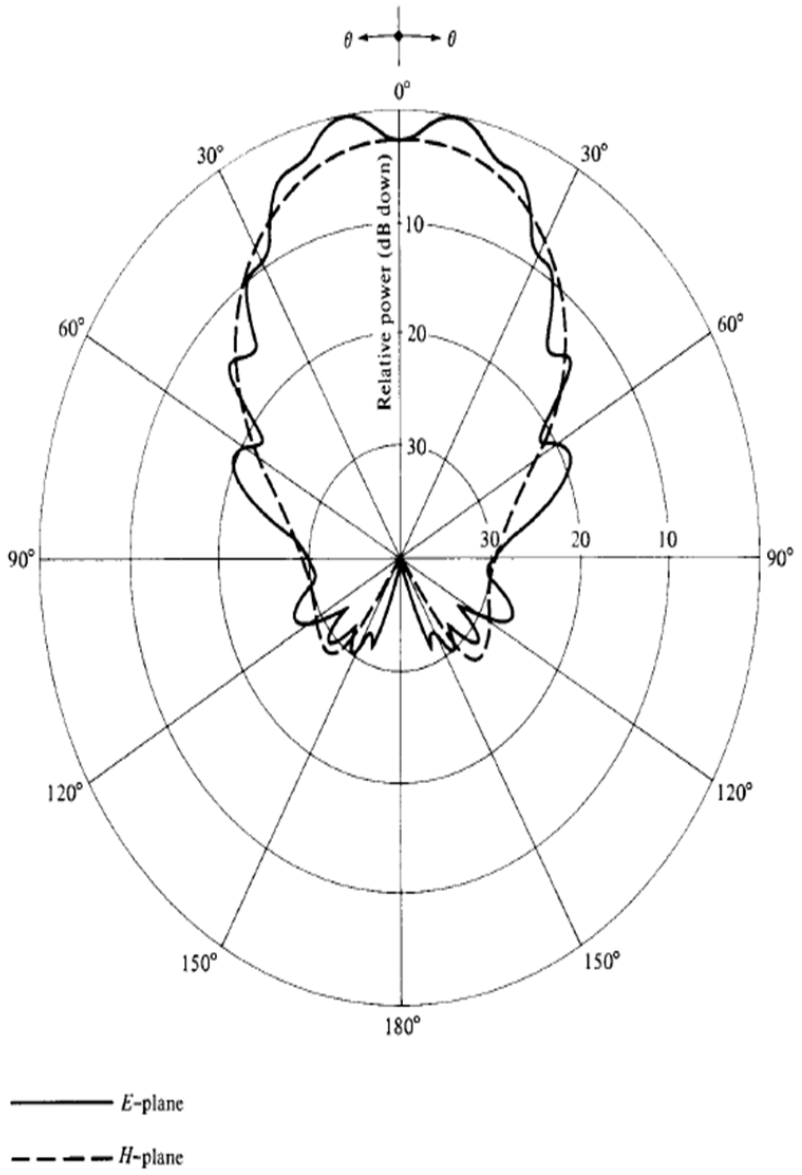

Figure 3.7: Radiation pattern of a pyramid horn antenna[58].

3.5.1 Pyramid Horn Antenna

The E plane and the H-plane horn antennas tend to focus the beam pattersn in the E and H plane respectively[58]. The pyramidal horn antenna combines the features of both the E-plane and the H-plane sectoral horns because it is flared in both the E and H plane. The results are thus combinations of the two other types of antennas. Figure3.7 shows the radiation pattern of the pyramid type antenna and the significant overlap of the two patterns seen in the chart verifies that this type of antenna focuses the beam pattern in both the E and the H plane. This makes the pyramid horn type antenna the choice best suited for this application as it would allow the capturing of the radiations in all directions.

The frequency response of the RF horn pyramid type antenna used as sensor to capture the radio frequency signals radiated as a result of PD activity shown in Figure 3.8. The antenna has a pass band between 1 - 2GHZ with a corresponding gain in the range 14.5 - 18 dB. The signals are then transferred to 2GHz bandwidth RS oscilloscope with a sampling rate of 10 GS/s via a low impedance cable to capture the fast varying RF signals with high fidelity.

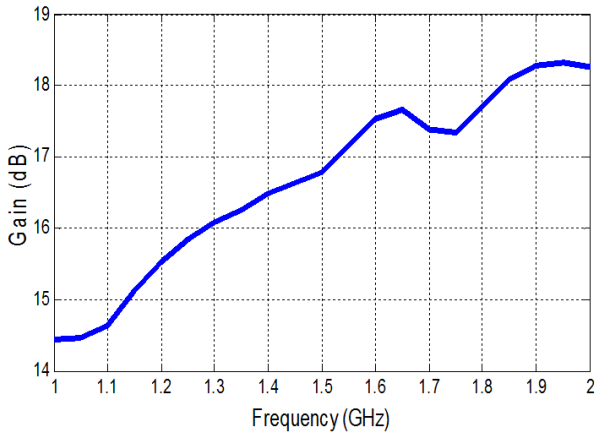

Figure 3.8: Frequency response of the selected pyramid horn antenna.

3.6 RF PD Data Patterns

The RF signature data representative of PD activity taking place within the insulator defects can be represented in several different forms.This includes time resolved

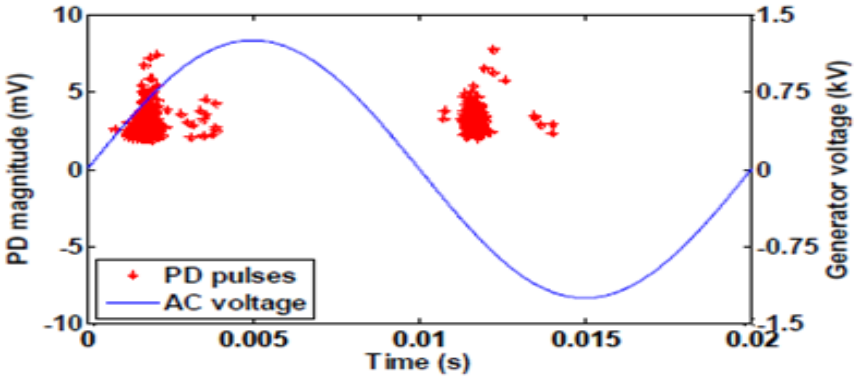

Figure 3.9: Phase Resolved RF PD signature[59]

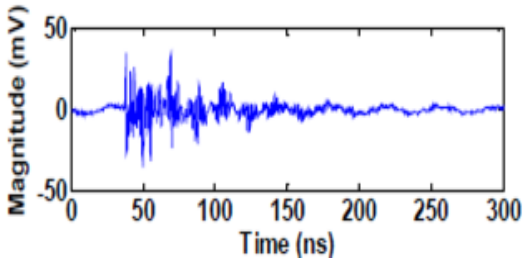

Figure 3.10: Time Resolved RF PD data [59].

patterns and phase resolved patterns. Figure 3.9 shows phase resolved PD pattern.

The data is acquired in relation to the waveform of the AC test voltage so a source of obtaining the power frequency waveform must be available for such a representation. The test voltage is considered constant and the phase angle of the test voltage is divided into small windows. The univariate distributions that are most commonly used for such a representation in which each of the PD pulses are quantified by their charge (q) and number of PD pulses (n) are [60]:

- $q_a \sim \phi$: average charge in each window vs ϕ.
- $q_p \sim \phi$): peak charge for each phase window vs ϕ.
- (n $\sim \phi$): number of PD pulses detected in each phase window vs ϕ.

Figure 3.10 shows time resolved PD pattern which represents the true shape of the discharge pulse. The magnitude of the discharge versus time is depicted in such plots.

In this work, the time resolved PD patterns are used a opposed to phase resolved plots. The reason behind this is that in a field setting it is difficult to obtain real

time reference voltage (60 Hz power frequency signal) so the time resolved PD data is the most convenient to obtain.

3.7 Experimental Test Setup

The samples are connected to high voltage end of the transformer at the cap and grounded at the pin end. A corona free test transformer (HIPOTRONICS Model T7150-20CF-L-G) is used, and the tests are conducted by applying up to 13 kVrms to the test samples. The inception of the PD activity is ascertained by using the classical PD measurement setup which along with a coupling capacitor is also a part of the circuit as shown in Figure 3.11. A wideband pyramid horn antenna is used as a PD sensor for capturing the RF signatures that are emitted as a result of PD activity within the defects in the samples.

The RF signatures are captured on a pulse by pulse basis using a time base of 200 ns. The terms "data", "signatures" and "signals" are used interchangeably in this thesis and all refer to these captured RF pulses. The RF signatures are captured with the with the aid a 2 GHz bandwidth oscilloscope. This RS oscilloscope has a sampling rate of 10GS/s which allows very fast varying components to be captured via a low impedance cable in an open loop arrangement. This data acquisition system is shown in Figure 3.12. The wideband antenna allows signals in the GHz range to be acquired with high fidelity.

In addition to the testing with single insulator discs, each of the three defective insulator discs is successively incorporated in strings of insulators. The resulting strings of two to four insulators are successively suspended on a tower structure similar to an overhead line high voltage transmission tower. The same test transformer is used here in order to apply higher test voltages of 30kV, 45kV and 65kV respectively to the the string with two , three and four insulator discs. The placement of the insulator sample is such that it is closer to the high voltage end.

.

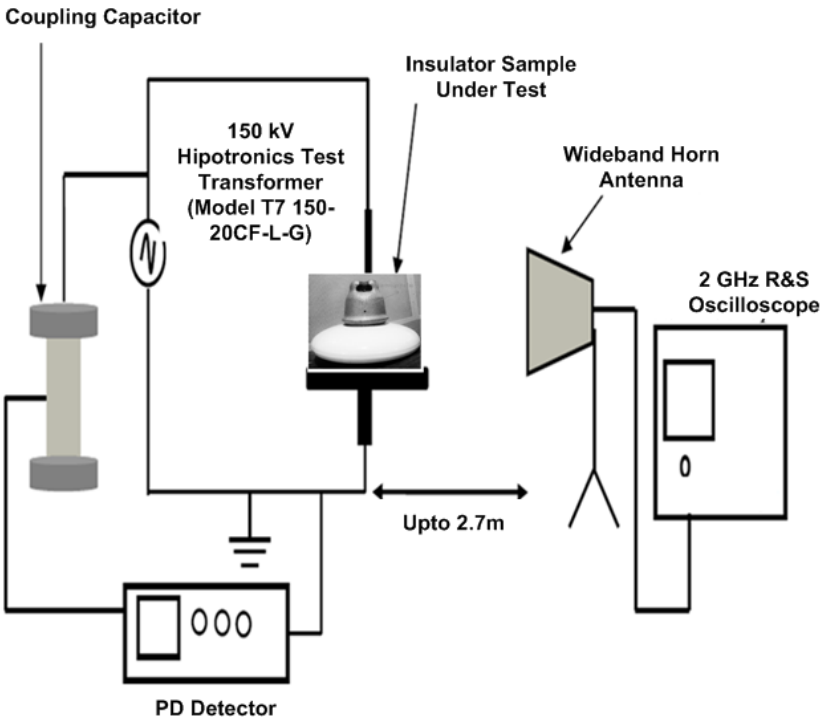

Figure 3.11: Test Setup Schematic illustrating the antenna, test transformer and PD level detector arrangement.

Figure 3.12: Data Acquisition System.

Figure 3.13: Test Setup showing the antenna, test transformer and the insulator sample under test.

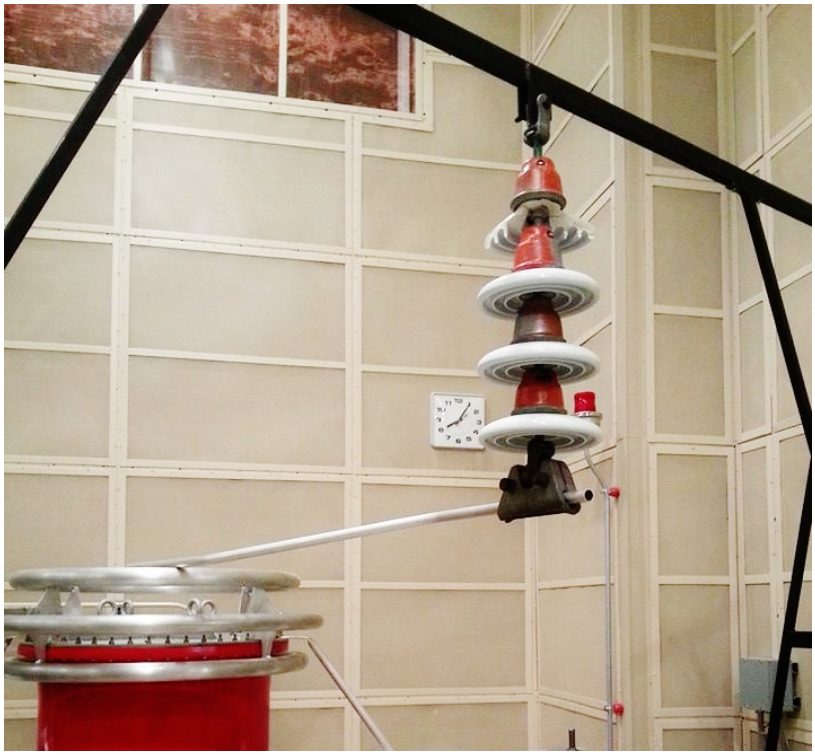

Figure 3.14: Four disc string with a completely broken insulator installed near the grounded end.

3.8 Defective Disc Position Within the Insulator String

In the previous section, when the insulator string was considered, the defective sample was always present near the high voltage end of the line. It is also important that consideration be given to variation of the position of the defective insulator sample within the string. Data corresponding to each position would be analysed for each different position in the time domain and the frequency domain. Figure 3.14 shows a four disc insulator hung from the tower structure with a broken insulator closest to the grounded end.

3.8.1 Electric Potential Distribution along a String of Porcelain Insulators

There exist stray capacitances of various forms such as between the insulator discs, between the insulator disc and the HV end and the ground. The non-uniformity of the electric potential along the insulator strings arises due to the fact that these different stray capacitances take on different values for different positions of the individual insulator disc. The electric potential or voltage distribution along the string of insulators is not uniform. The voltage along the insulator closest to the high voltage end is the highest and hence this insulator is stressed the most.This may suggest that the insulators near the high voltage end are the most likely to fail. However, this may not be always true because the defects are not solely developed as a result of operational stress. Indeed some insulator discs may have embedded defects during the manufacturing process and the high voltage stress might only serve to aggravate them. Hence defective discs may be present near the high voltage or near the grounded end and the need for their detection regardless of their position is important.

3.8.2 Test Procedures

The following four experiments are performed in order to extract the RF data corresponding to varying defective insulator positions.

- Experiments with four disc insulator string with a disc having a deliberately introduced crack near the high voltage line end.

- Experiments with four disc insulator string with a disc having deliberately introduced crack near the grounded end.
- Experiments with four disc insulator string with a completely broken insulator disc near the high voltage line end.
- Experiments with four disc insulator string with a broken insulator disc near the grounded end.

In each of the above experiments, the string of insulators was subjected to a sufficiently high voltage of 70kV to ensure a high signal to noise ratio of the captured RF signatures. The antenna was placed on a raised platform in order to capture the radiation in the radial direction to the defects, maintaining a distance of 2 meters from the string.

3.9 RF signatures obtained from PD activity

The time domain specimens of the RF signatures obtained for three different test samples and RF signatures due to corona are depicted in Figures 3.15 through 3.18. Simultaneous recording of PD level (apparent charge) through the PD setup validates that these signatures are radiated as a result of PD activity; in which the inception voltages are compared. Clear differences in the time domain can be seen between the signatures. This raw data comprising of the RF pulses is collected for a period of 5 minutes and corresponds to several thousand sample points.

3.10 Detection Sensitivity of the RF Antenna

In order to get a general idea of the detection sensitivity of the RF antenna the distance of the antenna from the test sample was varied and the corresponding detected signal amplitude was recorded for a range of distance values. The distance was varied from 0.7 meters to 2.4 meters. A general downward trend can be clearly observed as shown in the box plots in Figure 3.19 and Figure 3.20. Tables 3.1 and 3.2 tabulates the corresponding PD inception RF inception voltage where the RF signal inception voltage is always greater than the PD inception voltage.

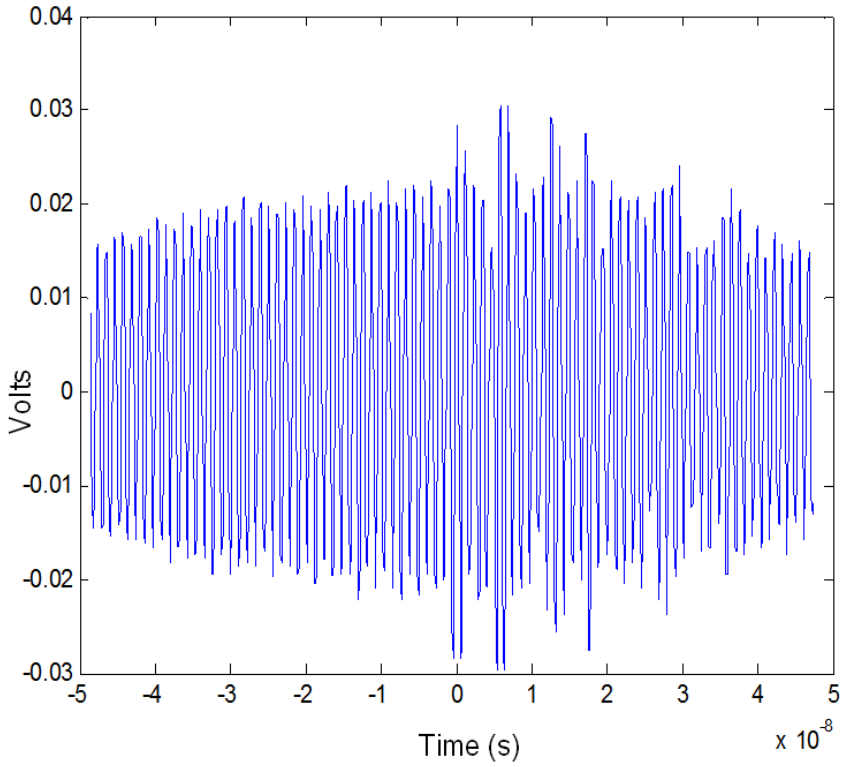

Figure 3.15: RF signature due to Corona.

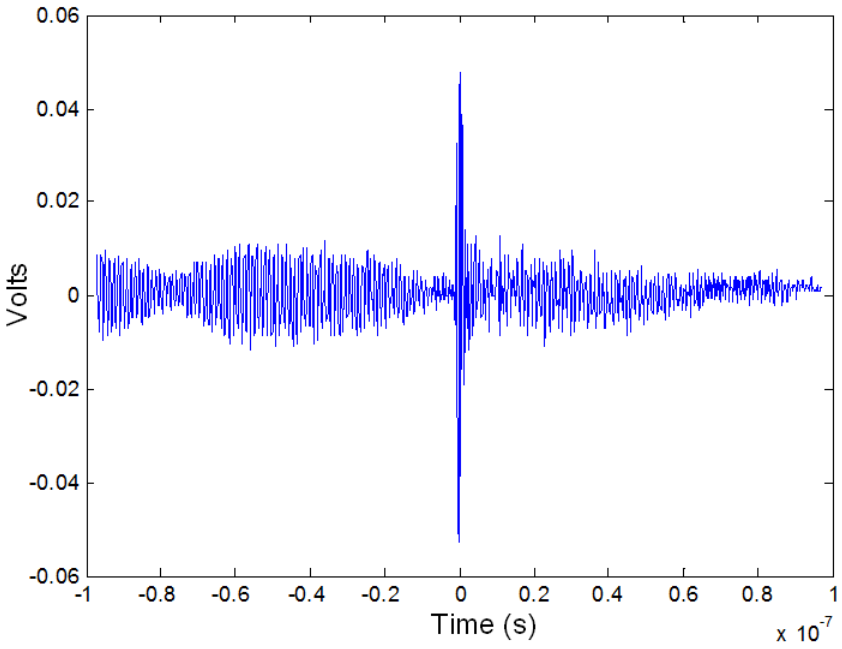

Figure 3.16: RF Signature corresponding to cracked insulator disc.

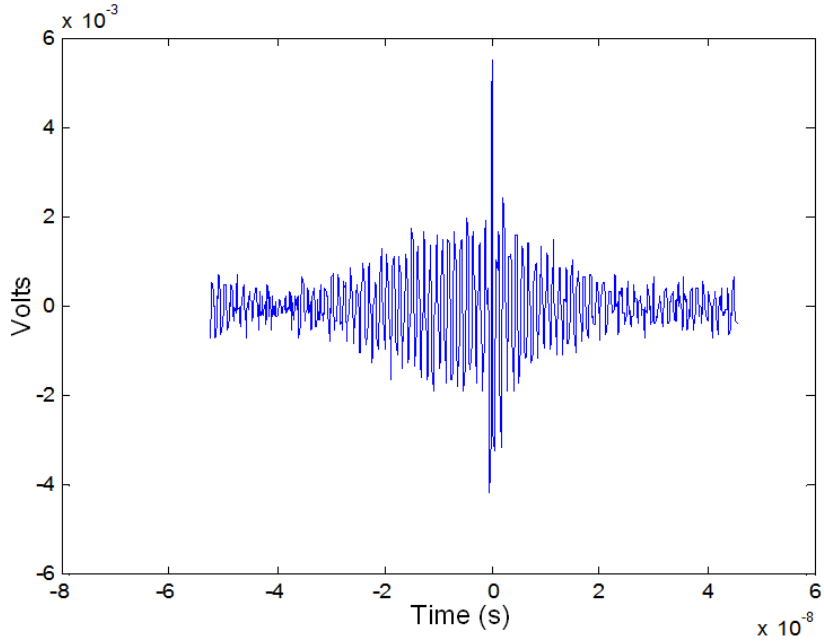

Figure 3.17: RF signature corresponding to broken insulator disc.

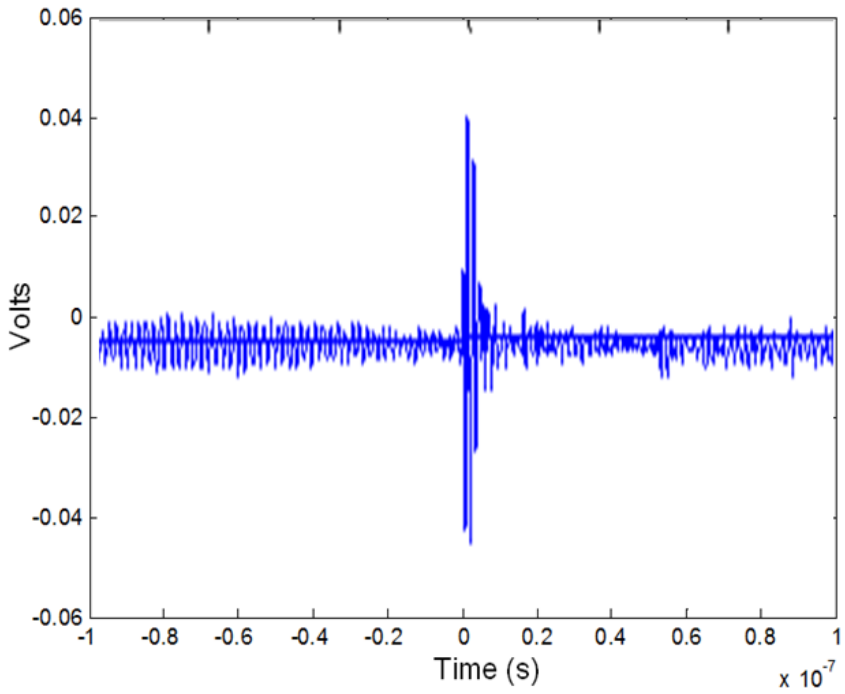

Figure 3.18: RF Signature corresponding to insulator with a hole through the cap.

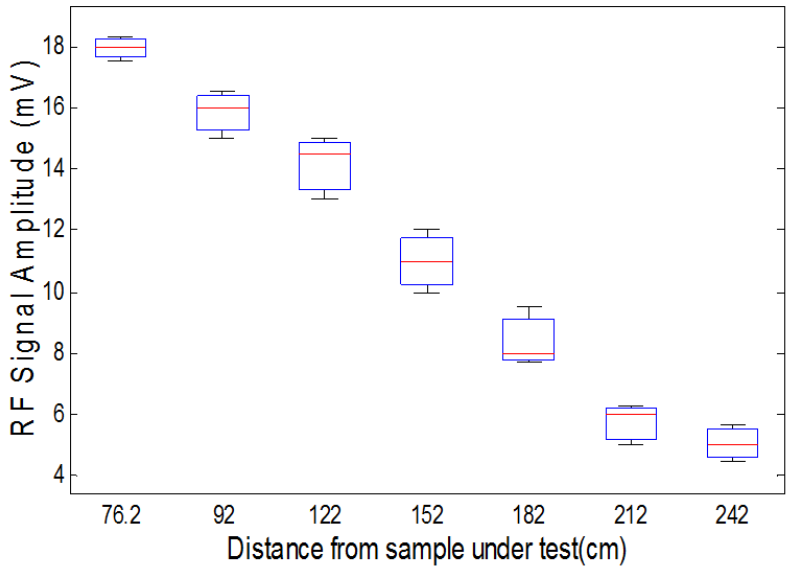

Figure 3.19: Box Plot showing the effect of variation of distance on RF signal amplitude for sample with a deliberately introduced crack.

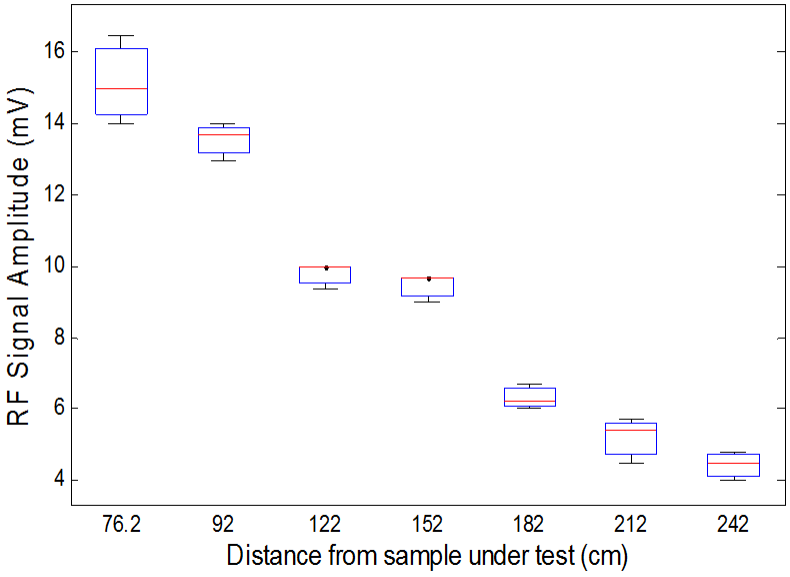

Figure 3.20: Box Plot showing the effect of variation of distance on RF signal amplitude for sample with a hole through the cap.

Table 3.1: Sensitivity of various measured parameters to the distance of the shell with an introduced crack from the antenna.

S. No	Distance (cm)	Apparent Charge(nC)	RF Signal Amplitude (mV)	PD Inception Voltage (kV)	RF Inception Voltage (kV)
1	76	0.5	17.0	5.0	5.5
2	92	0.6	15.0	5.0	5.8
3	122	0.8	13.0	5.5	6.2
4	152	1.0	10.0	6.0	6.6
5	182	1.9	7.7	6.5	7.0
6	212	4.0	6.3	7.0	7.3
7	242	5.7	5.7	7.4	7.6

Table 3.2: Sensitivity of various measured parameters to the distance of the broken shell from the antenna.

S. No	Distance (cm)	Apparent Charge (pC)	RF Signal Amplitude (mV)	PD Inception Voltage (kV)	RF Inception Voltage (kV)
1	76	50	15.0	7.5	8.0
2	92	66	14.0	8.0	8.9
3	122	100	10.0	8.5	9.6
4	152	152	9.6	9.5	10.1
5	182	200	6.2	12.0	13.0
6	212	250	5.4	12.5	13.5
7	242	400	4.8	12.0	13.8

As the distance increased the strength of the signal recorded by the oscilloscope decreased and so the signal to noise ratio also decreased. This general trend was observed for the two test samples that were considered for this experiment. This is satisfactory result because a distance of 2.4 meters is considered safe approach distance from clearance point of view for safety of the the operating personnel.

3.10.1 Effect of Variation of Applied Voltage on the Apparent Charge and the RF Signal Amplitude

The effect of the variation of applied voltage on the detected signal level is evaluated. The plots shown in Figure 3.22 and Figure 3.21 illustrate an upward relationship between the applied voltage and the RF signal amplitude recorded by the oscilloscope. As the applied voltage is increased the apparent charge injected into the sample also increases and this results in an increase in the RF signal voltage amplitude detected.

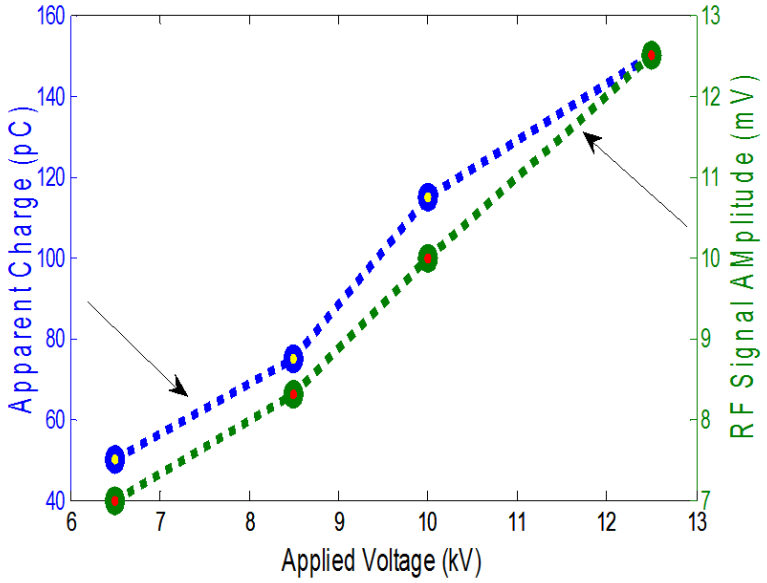

Figure 3.21: Effect of variation of applied voltage on the apparent charge and the RF Signal amplitude for a broken shell.

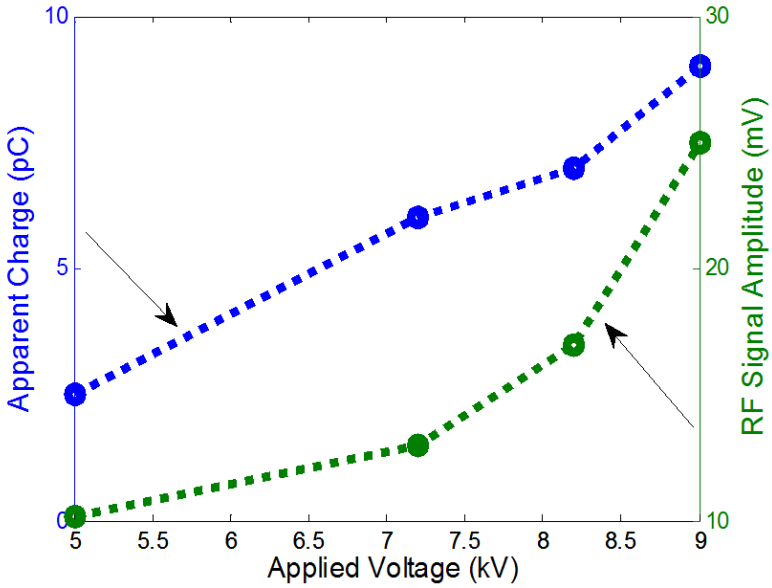

Figure 3.22: Effect of variation of applied voltage on the apparent charge and the RF signal amplitude for sample with a deliberately introduced crack.

Table 3.3: Minimum PD Level Detected and the Corresponding RF Signature Peak Amplitude Detected by the Antenna.

S.No	Minimum PD Level Detected (pC)	RF Signal Voltage (mV)	Inception Voltage (kV)
1	112	250	65.0
2	136	300	65.1
3	124	275	65.8
4	128	280	65.6
5	138	325	66.1

3.11 Minimum PD level detected by the Antenna for a string of insulators with four discs.

In order to test the system for real world application, a string of 4 insulators discs with one defective insulator sample is applied a voltage of about 66kV shown in Figure 3.14. The traditional technique for PD measurement based on IEC60270 and the RF method is applied simultaneously so that the the minimum apparent charge value corresponding necessary for RF detection may be known. The minimum PD level detectable by the RF antenna placed at a distance of 2 meters from the tower structure is noted. The simplest way to quantify the RF signature is noting its peak amplitude. Table 3.3 tabulates the minimum PD level detected and the corresponding RF signature peak amplitude detected by the antenna. This is important in order to make sure that the proposed technique is suitable detection technique in a field setting. A co-axial Mini-Circuits ZHL-42 amplifier is used in this experiment and any further experiments whenever the signal to noise ratio of the detected signal is observed to be very low.

Chapter 4

Classification Tools and Feature Extraction

This chapter presents the details of the classification tools (algorithms) that are used to classify the classes of defects are also a laid out. The wavelet packet decomposition technique which is also used as a feature extraction technique is described. In addition the feature extraction techniques and the extracted features are also discussed.

4.1 Introduction to Data Mining

In recent years, applications of data mining have increased tremendously owing to the huge amounts of data that is generated every second through almost every aspect of human activity. The goal of data mining is to discover patterns within these vast amounts of data and to uncover underlying relationships so some useful knowledge can be obtained. The data sets (called "instances") used in data mining applications comprise of a number of variables that are referred to as "attributes". The two different types of data are treated in radically different ways and depending upon these types the learning methods employed are also different.

4.1.1 Unlabelled Data and Unsupervised learning

The data that do not have any well assigned attributes are referred to as unlabelled data. The data mining techniques the are employed on such data types are referred to as unsupervised learning methods. Some widely used learning methods of this type include the clustering method and association rules. Clustering algorithms simply

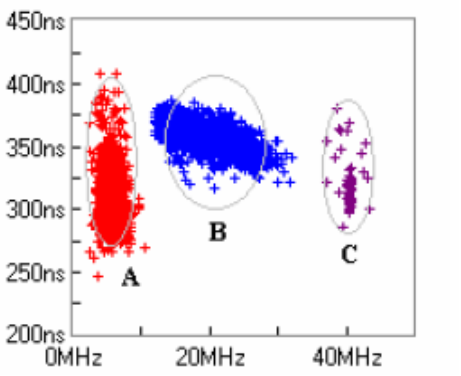

Figure 4.1: Unlabelled Data: Clustering Technique [61].

examine the data to form groups that are similar. Distinct clusters represent data that belong to different classes but the main goal here is simply to extract maximum information from the unlabelled data. Figure. 4.1 shows grouping of the internal discharge, noise and surface discharge according based on their extracted features.

4.1.2 Labelled Data and Supervised Learning

Labelled data have designated attributes associated with them. The objective is to learn from this data and predict the values of the attributes of the unseen instances. This technique is referred to as supervised learning. Depending upon the type of designated attribute the learning task can be categorised into classification task or simple regression task. For categorical attributes that is it must take one of a number of distinct values for example Hot,warm,cold etc , the task is referred to as a classification task. If on the other hand the designated attribute is numerical value such as fore casted weather for the next day, the learning task is referred to as Regression.

4.1.3 Classification

Classification of the data is the most widely employed data mining application[62]. The goal in classification is the prediction of a label for data that has not been seen before by the computer algorithm. The problem is to use the data attributes of the labelled data and to train the algorithm so that when a new data point is fed into the computer it can classify it based on the obtained knowledge from the previous data. The features are extracted for each of the different kinds of disturbances and based

on the features the algorithm is made to learn and adjust the internal parameters. When unseen data is input to the algorithm it can classify that data into the various possible disturbances. MATLAB is chosen as the platform to implement the procedure described earlier. MATLAB has built-in routines and functions for the analsyis and decomposition of the wavelet packet trees. In addition, MATLAB offers good capabilities for the the training and testing of feed-forward artificial neural network in one computational engine. Some of the methods that can be employed for the classification are explained at the very basic level here:

4.1.4 Nearest Neighbour Matching- Similarity based method

In this method the unclassified data point is identified as being most similar or closest in some aspect to the previously fed labelled data points (say 4 data points). If the newly fed data point has neighbours that have the labels "Hot", "Hot" , "Cold" and "Hot" then the unclassified instance can be classified to belong to the "Hot" class. As a generalisation of this method the number of neighbors to be assessed can be increased to achieve the best classification results. This general method is referred to as kNN where k is an adjustable parameter. The "closeness" between the data points is typically determined by using a certain distance function.

4.1.5 Neural Networks

Neural networks are complex modelling methods and quite popular tools used for classification problems. The idea of a neuron is borrowed from human brain neuron and a network of these neurons are interconnected and they are fed with labelled data that is used to train the network which can then be used to predict one or more outputs.

4.2 Classification Algorithm

Classification of the type of defects is mainly a combination of training where the algorithm is made to learn from the information presented to it and testing using new data where the unseen data is classified to identify the 4 classes elaborated earlier. An excellent review of the various techniques for classification of PD sources is presented

in [62]. Both the statistical and the spectral features were used in order to compare the performance of the classification algorithms which are briefly discussed next.

4.2.1 Artificial Neural Network (ANN)

Back Propagation algorithm is the basis of the ANN technique thats employed after successive testing with different algorithms. The architecture comprises of a two layer network where the two layers are the hidden and the output layers. All of the layers are made up of numerous neurons themselves with the input layer having 513 neurons corresponding to each of the data points in the DFT of the signatures. For the data obtained from the single insulator discs the ANN is trained with the hidden layer having 300 neurons and the output layer having 4 neurons. For the data obtained from the string of insulators input layer having 110 neurons corresponding to each of the data points in the DFT of the signatures. The hidden layer has 10 neurons and the output layer has 4 neurons. Every neuron has an associated input, bias, an activation function and an output. The input x is weighted by a weighting function W_{ij} as shown in Figure 4.2.

The total activation is determined by adding the weighted inputs with bias b. The hidden layer output is dependent on its activation function which for this particular network is a sigmoid function. In a similar manner the non-linear sigmoid function is used to calculate the output in the output layer. The ANN architecture that was employed for the statistical features is similar to the architecture for FFT features, the differences being that there are only 6 inputs as opposed to 110 inputs.

4.3 Wavelet packet Decomposition

Wavelet Packet decomposition (WPD) is an extension of the discrete wavelet transformation. In the discrete wavelet transform only the approximation coefficients are passed through high pass and low pass filter to yield the coefficients at a given level. In wavelet packet decomposition both the the approximation as well as the detail coefficients are further decomposed, this results in a whole binary tree formation. Translated and scaled wavelet packet functions $W_{j,k,n}$ are the basis of the wavelet packets. Figure 4.3 and Figure4.4 demonstrate the implementation of a wavelet packet

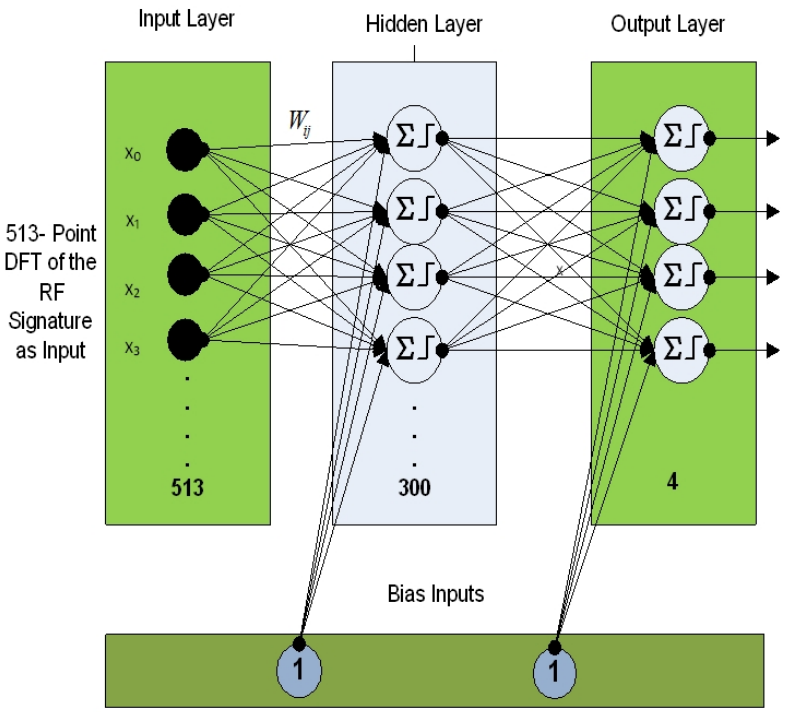

Figure 4.2: Artificial Neural Network Architecture.

decomposition algorithm and the resulting tree like structure respectively.

$$W_{j,k,n}(t) = 2^{\frac{j}{2}} W_n(2^j t - k) \tag{4.1}$$

where j describes the scaling index and k describes the translation shift. The index n describes the number of oscillations. The wavelet packet tree is formed using a fast decomposition algorithm which is adapted from the pyramid algorithm, also used for obtaining the discrete wavelet decomposition.

4.4 Feature Extraction

4.4.1 De-noising of the collected PD data by Wavelets

The acquired RF signals are corrupted with background noise hence de-noising the data is crucial in order to extract suitable statistical features. The knowledge of the signal itself will be used to mitigate the noise since the RF antenna DAQ is an open loop system. Some of the methods for open loop noise mitigation include the use of wavelets, filtering and pulse averaging. Wavelets will be employed here for the purpose

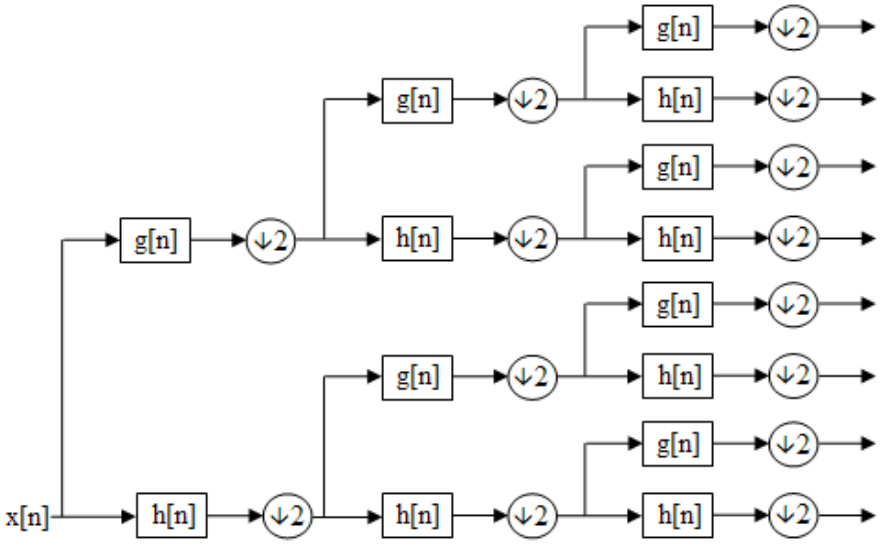

Figure 4.3: Wavelet Packet Decomposition algorithm implementation using discrete high and low pass filters.

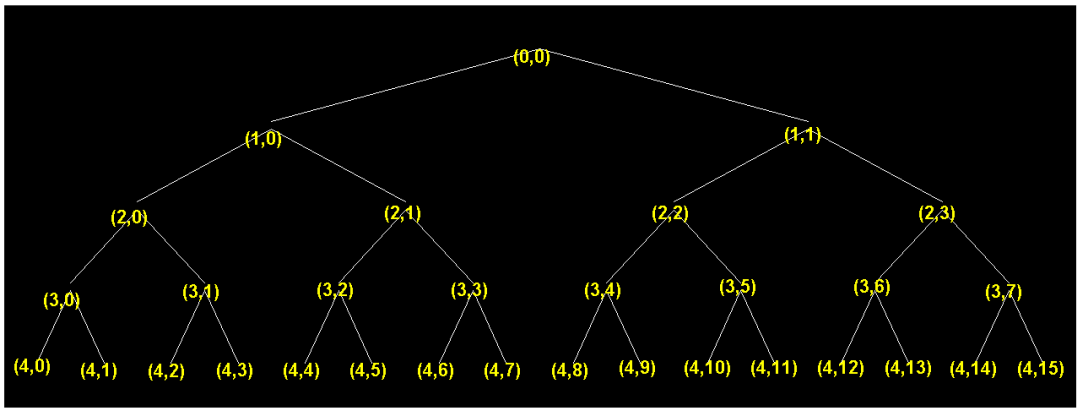

Figure 4.4: Wavelet Packet Tree for a 4-level decomposition.

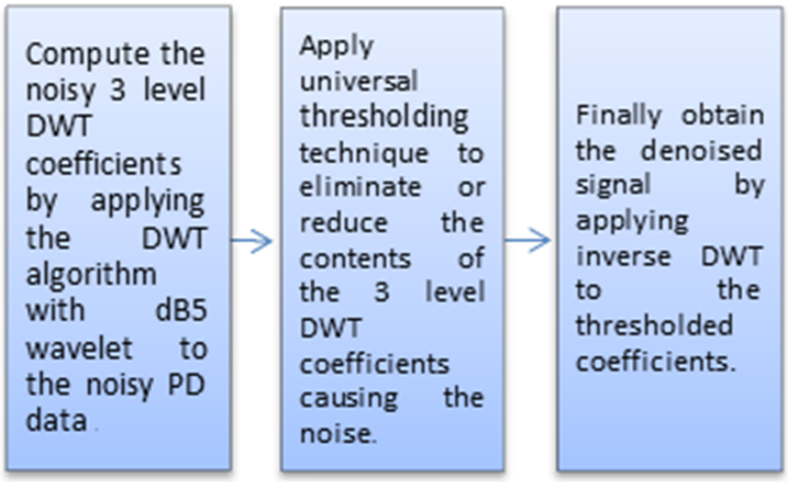

Figure 4.5: Flowchart illustrating the de-noising steps.

of de-noising the data. The Discrete Wavelet Transform (DWT) for any function f(t) and its inverse transform is given in [63]. Primary motive here is to reduce the noise from the corrupted PD data. This can be achieved by applying a procedure proposed by Johnstone [64] and Donoho [65] which is shown by the flowchart in Figure 4.5.

Here, the threshold refers to an estimation of the noise level. The data that is larger than the threshold is considered to be the actual signal whereas the values falling lower than the threshold are considered to be the noise. Thresholding algorithm plays an important role in de-noising the data. The technique that is employed here is called the universal threshold proposed by Donoho and Johnstone[66] who showed that the risk associated with this thresholding method is low enough to meet the demands of a wide variety of applications. The threshold values obtained by this method are given in [67].

4.4.2 Statistical Features

The statistical features are comprised of six statistical measures including mean, mode, media, kurtosis, skewness and standard deviation which are calculated for each of the 200 data points. The skewness measures the degree of asymmetry with respect to the sample mean. The skewness of a normal distribution is zero. Skewness S of a discrete signal x is defined by Equation (4.2):

$$S = \frac{\sum_{i=1}^{N}(x_i - \mu)^3)}{(N\sigma^3)} \tag{4.2}$$

Kurtosis of a discrete distribution function x measures how peaky the distribution is with respect to the normal distribution. Mathematically it is given by Equation (4.3).

$$K = \frac{\sum_{i=1}^{N}(x_i - \mu)^4)}{(N\sigma^3)} \tag{4.3}$$

where μ and σ are the mean and the standard deviation of x_i.

4.4.3 Spectral Features

The spectral features are comprised of the discrete Fourier transform (DFT) of the signatures given by Equation (4.4). As a result of DFT operation the signals are resolved into their frequency domain counterparts and hence the noise components can easily be spotted, rendering the de-noising process unnecessary.

$$X(k) = \sum_{n=0}^{N} x(n) e^{\frac{-j2kn}{N}} \tag{4.4}$$

where K = 0,1,2, N-1.

Owing to the stochastic nature of the PD signals, normalized FFT plots of 20 random samples each for three different classes are shown in Figures 4.6 through 4.9. The spectral density for the insulator with a crack is spread over a wide range, between 1.5 GHz and 2.5 GHz, with the largest component at around 1.7 GHz; whereas, for the broken insulator this spread was not observed. This is attributed to the dimension of the crack that was deliberately introduced in the disc. The size and shape of this crack determines the amount of radiated electromagnetic waves due to PD activity within the defective disc, hence higher magnitude frequency components are radiated that fall in a wide bandwidth range.

Similarly a unique spectral density plot is obtained for the case of corona noise with components in the 800 MHz and 2 GHz band. It can be concluded that distinct differences are present in the spectral energy distribution for each of the different classes of defects. Thus these spectral features could be good candidates to serve as

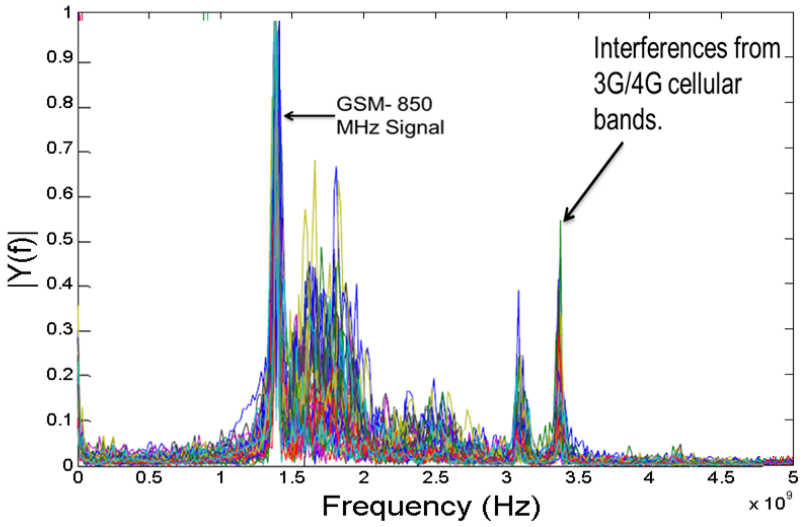

Figure 4.6: FFT Plots for 50 corona signal samples.

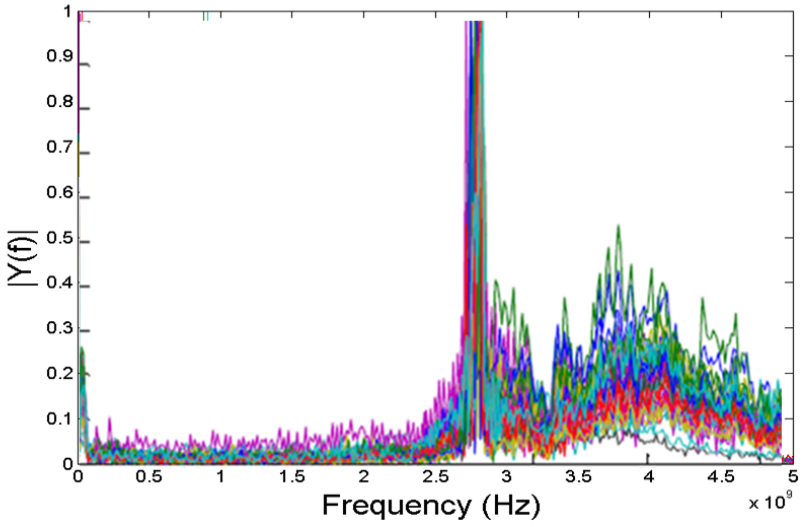

Figure 4.7: FFT Plots for 50 signal samples for a cracked insulator disc.

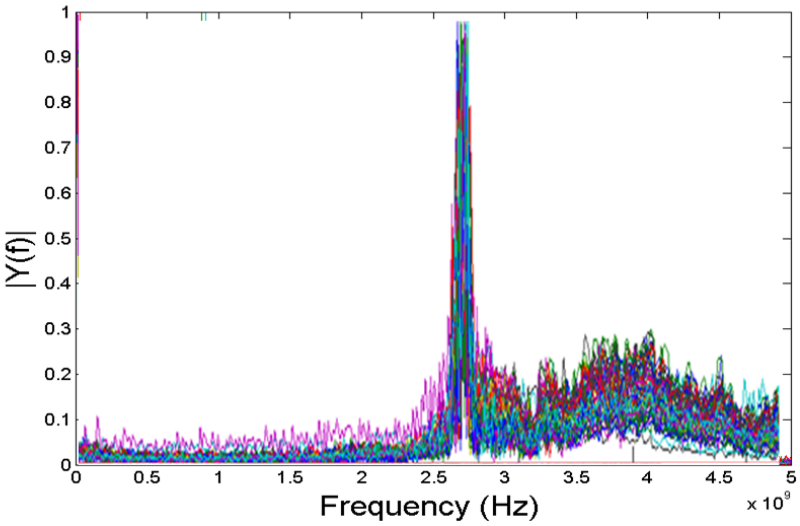

Figure 4.8: FFT Plots for 50 signal samples for an insulator with a hole through the cap.

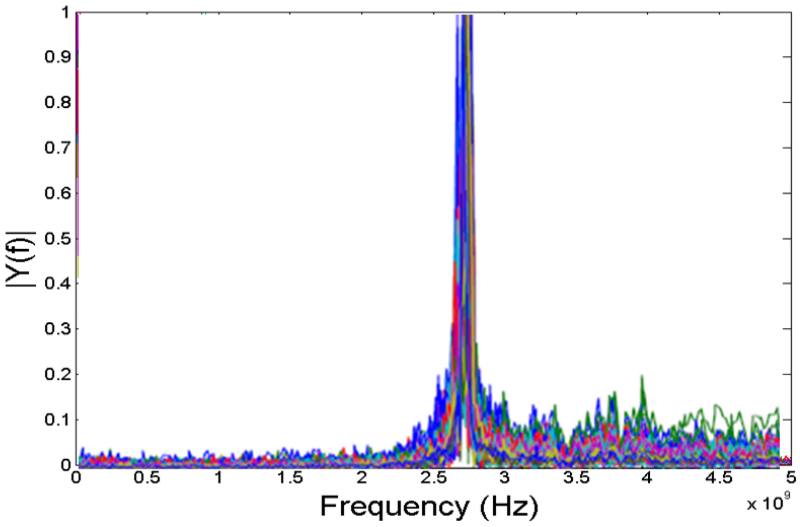

Figure 4.9: FFT Plots for 50 signal samples for a broken insulator.

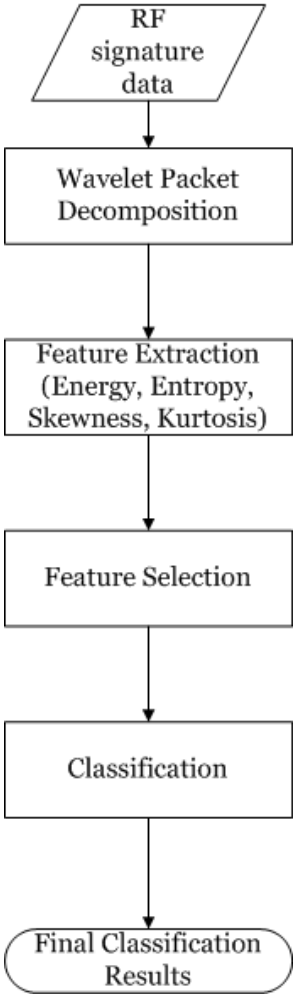

Figure 4.10: Flowchart illustration of classification of ceramic insulator defects using wavelet packet based features.

input feature vectors for ANN. The classification of the defects is based on the spectral and statistical features and a performance comparison was made of two approaches. Earlier in the paper, it has been established that different defects contribute to a different distribution of the spectral energies. Thus, these differences in the features are sensed by the neural network classification, allowing the network to alter its parameters based on the training data. Therefore, when presented with a large quantity of unseen test data, the algorithm is able to classify them with a high accuracy.

Table 4.1: Selected Features to be Fed into the Neural Network.

	Node 1	Node 2
Node Energy	(3,5)	(4,11)
Node Kurtosis	(5,7)	(2,3)
Node Skewness	(1,0)	(0,0)
Node Entropy	(2,0)	(3,0)

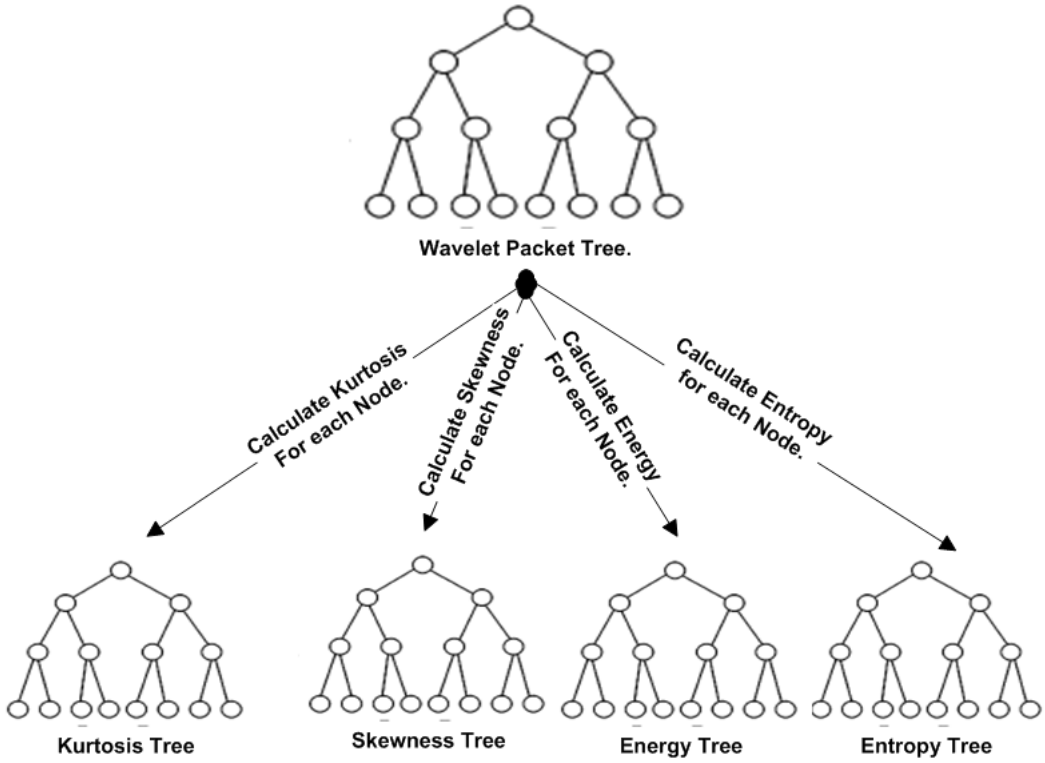

Figure 4.11: Features Extracted from the WPD tree.

4.5 Feature Extraction Based on Wavelet Packet Decomposition coefficients

The flowchart in Figure 4.10 illustrates the procedure for classification of the ceramic insulator defects using features extracted from wavelet packet decomposition. Wavelet based features allow the capture of the local time varying features because of the presence of additional time information, as opposed to the Fast Fourier Transform (FFT) which captures the global features. This would result in better discrimination between the classes, leading to a higher recognition rate.

4.5.1 Entropy

Entropy refers to the Shannon entropy of the discrete distribution. Consider a discrete signal X [x_1, x_2 , x_n], the entropy of this signal is given by Equation(4.5).

$$H = -x_i \sum X_i log(x_i) \tag{4.5}$$

Entropy is a measure of uncertainty or disorder within a system. A signal which is more chaotic will generate a larger value of entropy and vice versa. The entropy values of every node within the wavelet packet tree is computed and serves as one of the features.

4.5.2 Energy

The extraction of the local time frequency features is made possible by the use of wavelet packet decomposition. The wavelet node energy can be defined as:

$$e_{j,n} = |w_{j,n}|^2 \tag{4.6}$$

where $w_{j,n}$ is the two parameter array of wavelet packet coefficients corresponding to one node (j,n) in the decomposition tree.

4.5.3 Skewness and Kurtosis

Skewness and kurtosis have been defined in earlier chapters. Here the kurtosis and skewness values are computed for each node and serve as the features.

4.5.4 Feature Selection

In order to mitigate the issues caused by the curse of dimensionality [62] it is critical to reduce the size of the feature space. Also it is very important that a high degree of separability be achieved between the data points. Thus a method has to be adopted to maximise the separability within the class and as well as between the classes. A feature selection method is thus adopted which is based on the computation of within-class scatter S_w and the between classes scatter S_b values for every node of the wavelet packet tree. A ratio of the two quantities B is calculated and the nodes are ranked based on the largest values of this ratio. A higher value of the ratio indicates

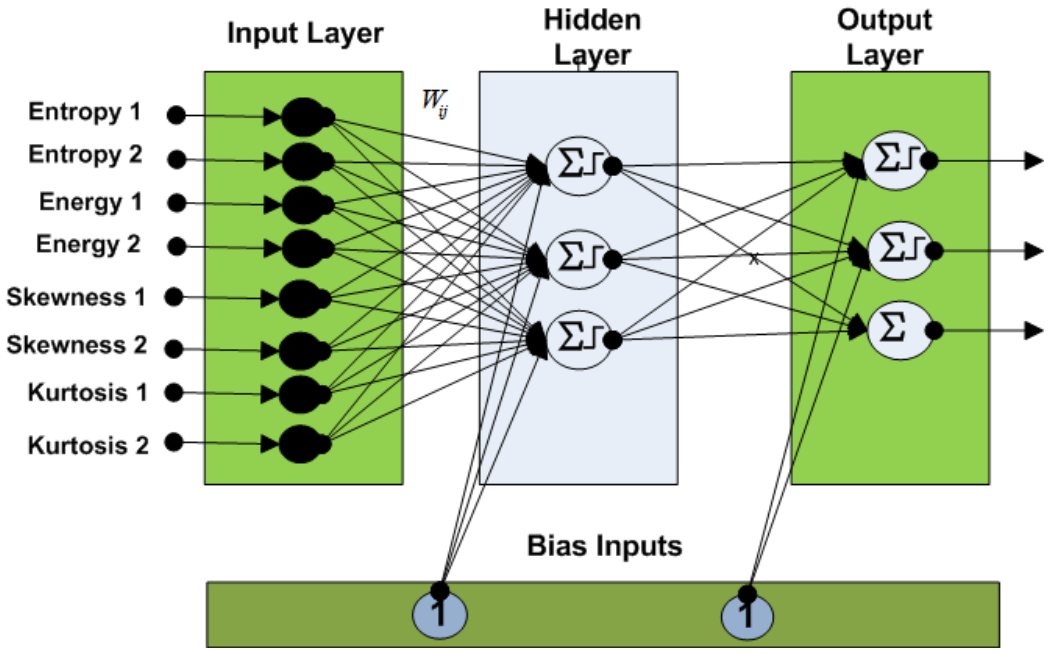

Figure 4.12: ANN architecure for the WPD feature set.

a high between class scatter S_b and a low within class scatter S_w. The two highest ranked nodes are selected and the features extracted from these nodes are to be input to the classifier for further classification.

$$B(j,n) = \frac{S_b(j,n)}{S_w(j,n)} \tag{4.7}$$

where the two quantities S_w and S_b are defined according to the Equations (4.8) and (4.9).

$$S_w(j,n) = \sum_{c=1}^{L} \frac{N_c}{N} \sigma_c(j,n)^2 \tag{4.8}$$

$$S_b(j,n) = \sum_{c=1}^{L} \frac{N_c}{N} (\eta_c(j,n) - \eta(j,n))^2 \tag{4.9}$$

In the above two Equations N_c represents the total number of samples belonging to class c. N is the total number of samples. $\sigma_c(j,n)^2$ represents the node variance of the selected features for class c. $\eta_c(j,n)$ and $\eta(j,n)$ represent the features mean values at a node for class c and all of the samples respectively.

Chapter 5

Results and Discussion

The extracted features are used to train and test the classifier ANN as described in Chapter 4. The classification performance results are presented for the single disc and the string of insulators using statistical, FFT and WPD based features. In addition the classification performance corresponding to variation of the defect location within the string is presented.

5.1 Classification Results for Single Defective Discs

In this study the feasibility of using a non-contact monitoring system for detecting the defects in ceramic insulators based on their RF signatures was investigated. The method not only provides the possibility of detecting the PD activity or the defect, but also the classification of the specific insulator defect which allows identifying the root of the problem for PD activity. A high recognition rate of over 91% was achieved when the normalized DFT components of the distinctive RF signatures obtained for each defect were used as training vectors for the ANN. The Table 5.1 presents the complete classification results for each of the 4 classes, where the first class represents corona due to point to plane setup, the second class corresponds to a cracked insulator sample, followed by a sample with hole through the cap and finally a completely broken insulator constitutes the fourth class. A much poorer classification performance may be observed for statistical features as shown in Table 5.2

Table 5.1: Classification Results for FFT Based Features.

	Average Recognition Rate	Maximum Recognition Rate
Class 1 Rate	100%	100%
Class 2 Rate	85%	92%
Class 3 Rate	87%	98%
Class 4 Rate	93%	100%
Overall Rate	91%	95%

Table 5.2: Classification Results for Statistical Features

Overall Average Recognition Rate	Overall Maximum Recognition Rate
63%	70%

5.2 Classification Results corresponding to String of Insulators with Defective Discs

Figure 5.1 shows the background noise signal which has amplitude of about 2mV. Results for de-noising of the data for statistical features are depicted in the Figures 5.2(a) - 5.2(c). The de-noising clearly removes the component as can be seen by the final de-noised signal and the close similarity of the residual signal with the background noise. Applying the de-noising algorithm is projected to improve the classification results corresponding to statistical features and this would be demonstrated in the results for string of insulators with defected samples using statistical features.
The 200 normalized DFT vectors corresponding to each data point were obtained for all of the classes. The FFT for the four different classes for 2-disc string is shown in Figure 5.3. The 200 feature vectors were split equally into 100 vectors each and were used for training and testing of the algorithms. In 900 MHz-2 GHz frequency range, no interference is observed and higher magnitude frequency components are seen for all the classes. For instance the insulator disc with a deliberately introduced crack can be seen to have high magnitude components at the 1150 - 1250 MHz. Similar observations can be made for the broken insulator disk which has somewhat lower magnitude components.

The testing and training was performed for a total of 10 times using data from tests with 2, 3 and 4 discs. Table 5.3 and Table 5.4 show the average classification results of the algorithm for statistical and spectral features. With the FFT based features

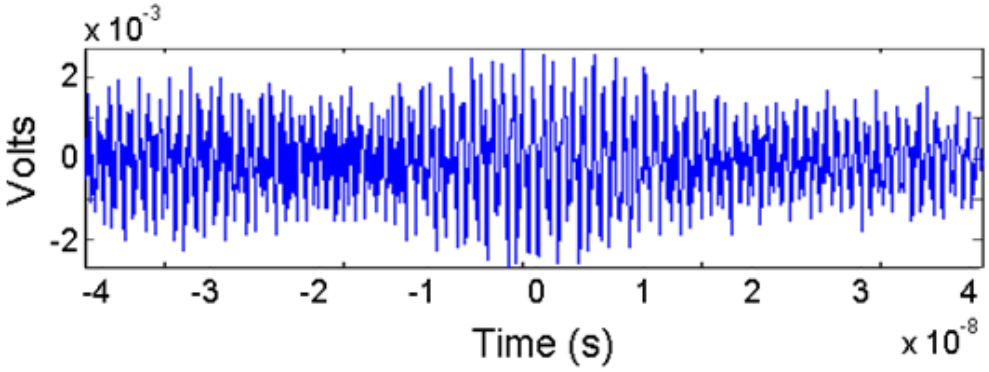

Figure 5.1: Background Noise.

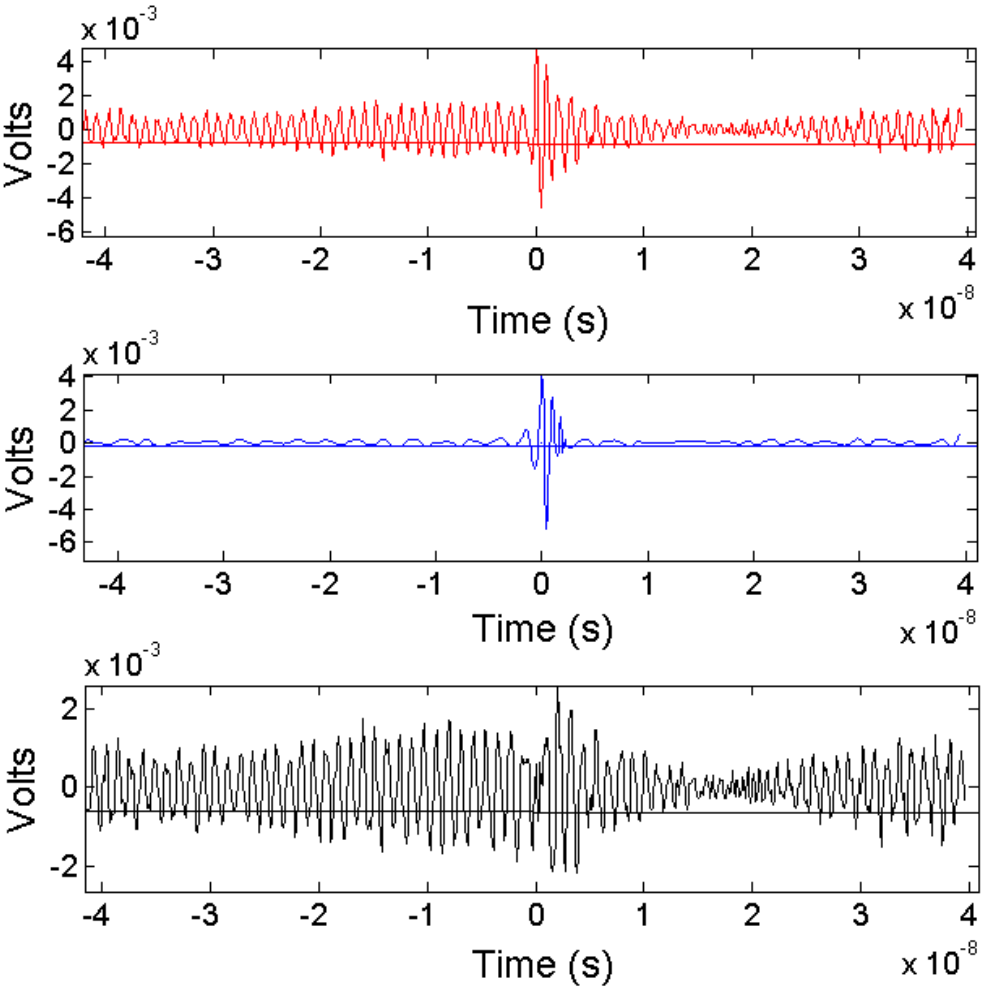

Figure 5.2: (a) RF signature corrupted with noise (b) De-noised signal (c) Residual Signal.

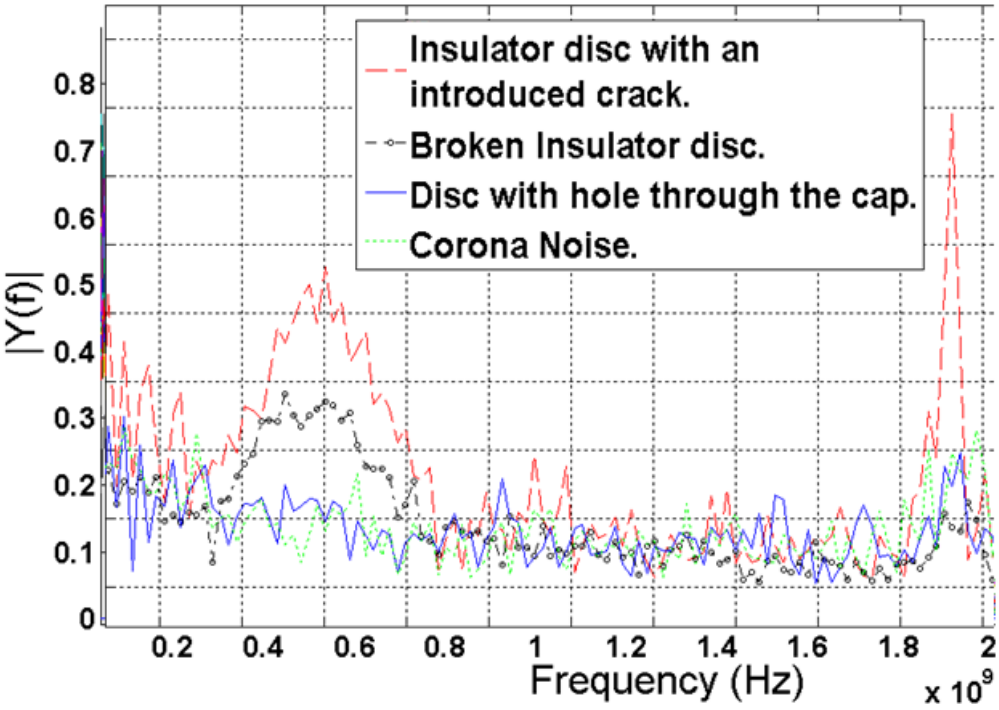

Figure 5.3: Normalized DFT Plots of features of interest for different defect conditions in a 2 disc string.

Table 5.3: Classification results for Statistical features.

Number of healthy insulators in string	Class1	Class 2	Class 3	Class 4	Overall Rate
1	78	98	92	75	86
2	75	96	73	89	84
3	85	75	65	92	79

the ANN performs satisfactorily having all their recognition rates above 90%. In this study the feasibility for detection and classification of defects in string of insulators is analyzed using ANN algorithm. It was seen that FFT based features demonstrate a better performance compared to the statistically based features. The best performing combination of features and algorithm is the ANN model with FFT based features with recognition rates as high as 95%. The technique discussed in this paper has the potential to provide a robust and cost-effective patrolling tool for the utilities to evaluate their aging ceramic insulators.

Table 5.4: Classification results for FFT based features.

Number of healthy insulators in string	Class1	Class 2	Class 3	Class 4	Overall Rate
1	89	89	93	94	91
2	95	96	90	96	95
3	93	90	93	100	94

Table 5.5: Classification results corresponding to the variation of position of the defects within the insulator string.

	Average Recognition Rate	Maximum Recognition Rate height
Class 1 Rate	91	92
Class 2 Rate	92	95
Overall Rate	92	93

5.3 Variation of Insulator Disc Position

Having acquired all the data for the 4 different experiments as outlined in the Chapter 3, the data is transferred from the memory of the oscilloscope to the PC. This comprises the labelled data set which is used to extract features based on Wavelet packet decomposition as explained in earlier section. The extracted features are energy, entropy, kurtosis and skewness. In order to prove the robustness of this technique the classifier using these features must be able to classify the defects based on the type of the defect and the position of the defective sample should have no bearing on the classification. The classification of the extracted features is carried out using Artificial Neural Network Algorithm. The data corresponding to each of the insulator positions is combined together to form one class so that the possibility of identification of a defect type regardless of its position can be established.For this experiment only two insulator defects the broken insulator sample and cracked insulator sample would be considered. Therefore this becomes a two class problem. Table 5.5 tabulates the results of this classification.

5.4 Results for WPD based features

Only the RF signatures due to the defective insulators are considered and corona as a separate case is not considered. Corona is relatively easier to identify as was demon-

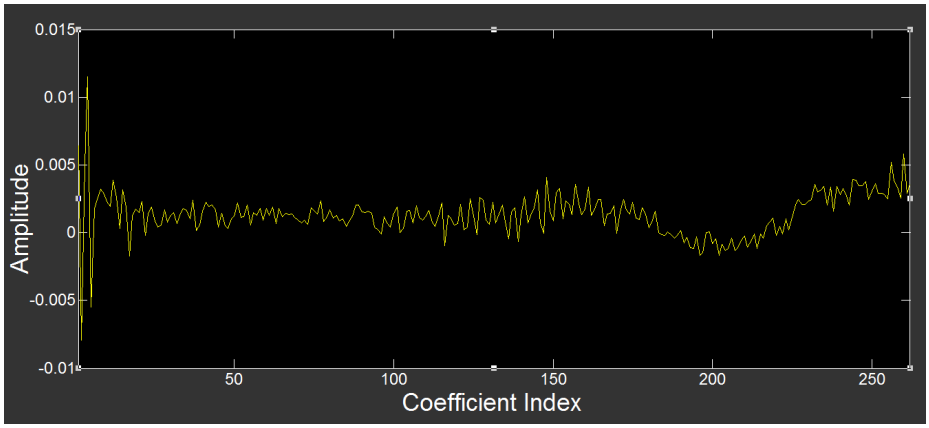

Figure 5.4: Wavelet Packet coefficients for broken insulator at node (2,3).

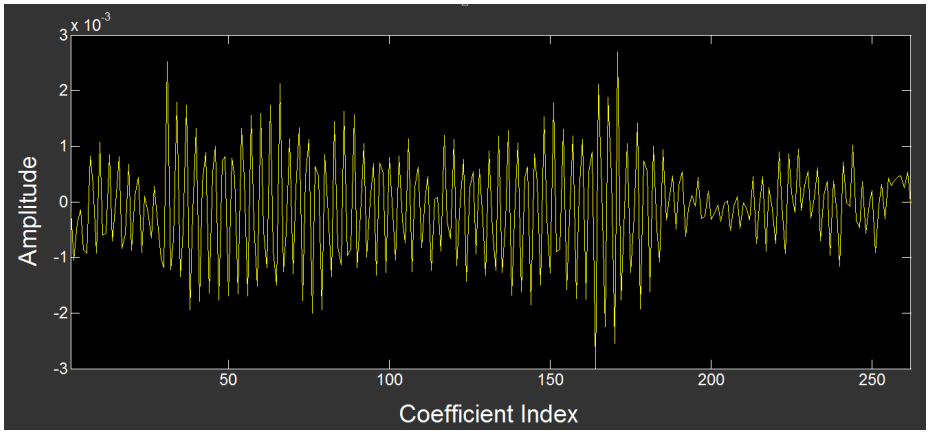

Figure 5.5: Wavelet Packet coefficients for insulator with a hole through the cap at node (2,3).

strated through the previous classification results. Considering only three types of PD cases reduces the work for the classifier and results in higher degree of classification for the other three PD cases. Two best nodes are selected according to the selection criteria described earlier for each of the four features which are tabulated in table. Figure 5.4 and Figure 5.5 show the wavelet packet coefficients at node (2,3) which is also one of the nodes that were selected for feature extraction.

The feature clusters are plotted in Figure 5.6 and a clear separation can be observed between the different classes and points of the same class have least scatter. This shows the effectiveness of the proposed feature selection procedure based on minimizing within-class scatter and maximizing between-class scatter. Further, the capability of the feature selection technique to select the best features can be demon-

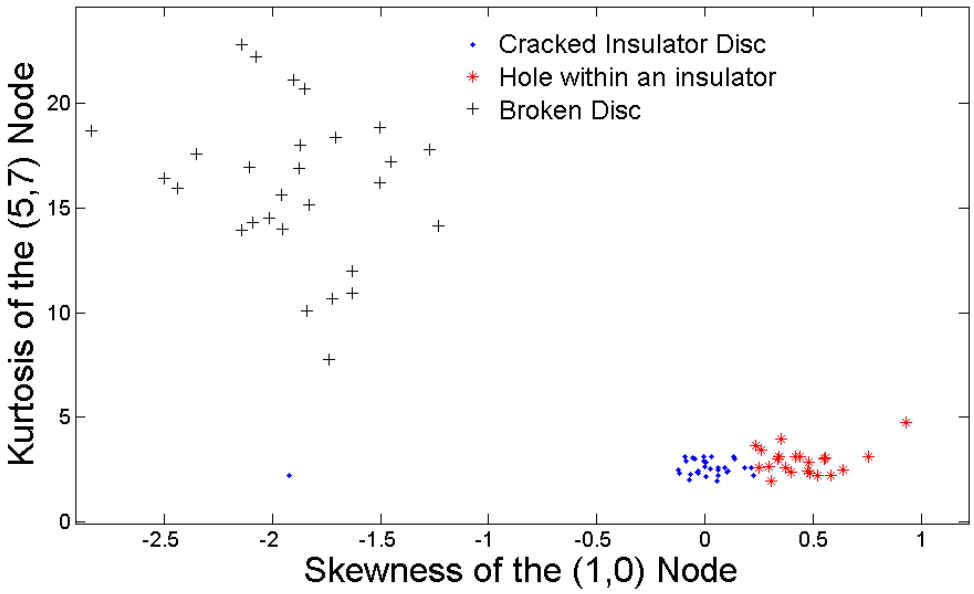

Figure 5.6: Cluster plot for skewness versus kurtosis.

strated through the Figures 5.7 and 5.8. These figures show the kurtosis plots for 15 different samples corresponding to the two best nodes selected through the feature selection method. Figure 5.7 shows the kurtosis values for the best node, (5,7) according to the feature selection procedure of the decomposition tree and Figure 5.8 shows the kurtosis values for the second best node (2,3). As can be observed from the plots the kurtosis values for each defect demonstrate a high degree of scatter and there is nearly no overlap between the kurtosis values for the broken disc and the other two types of defects. The cracked sample and the disc with a hole through the cap also can be easily discriminated even though some of the points are quite close to each other. The second best node (2,3) exhibits somewhat more overlap as compared to the best node, however majority of the sample points in this case like the previous case are well separated.

The 50 samples belonging to each of the three classes where class 1 is the cracked insulator sample, class 2 is the sample with a hole through the cap and the class 3 is the broken insulator sample are used for a total of 150 samples. Out of these, 108 samples are used for the training of the neural network and the remaining 42 samples are randomly selected from the three classes to test the trained network. With the selected features, the neural network training converges after 51 epochs and an over

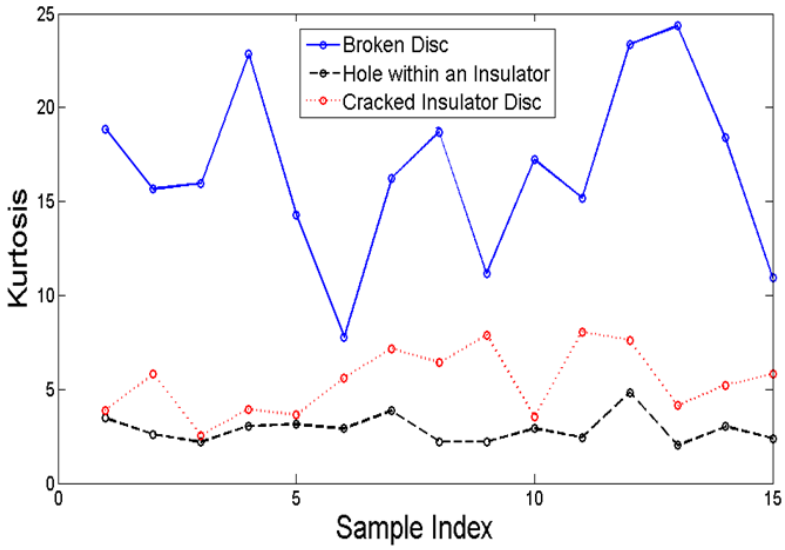

Figure 5.7: Values of Kurtosis for WPD coefficients of the samples at Best Node (5,7).

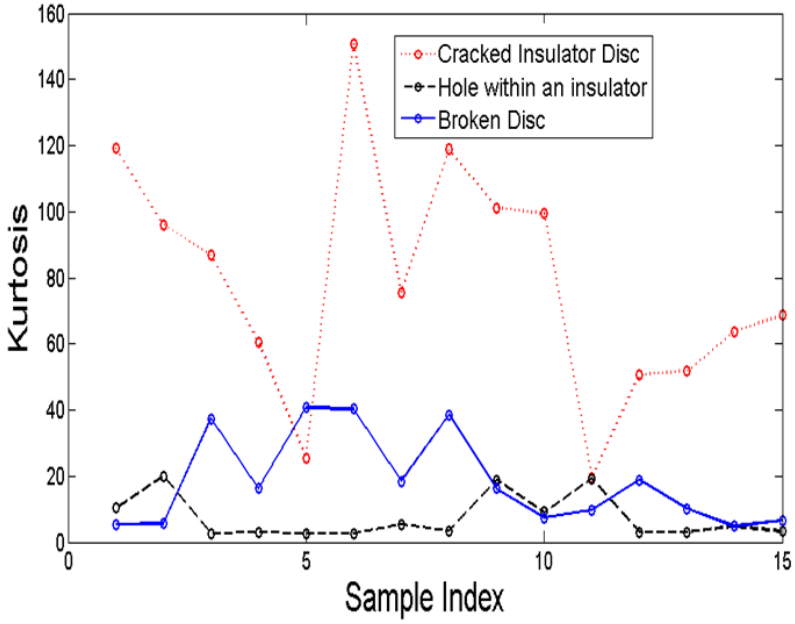

Figure 5.8: Values of Kurtosis for WPD coefficients of the samples at 2nd Best Node (2,3).

Table 5.6: Classification Performance for single disc PD RF signatures using WPD based features.

	Average Recognition Rate	Maximum Recognition Rate
Class 1 Rate	96	97
Class 2 Rate	97	100
Class 3 Rate	99	100
Overall Rate	97	98

Table 5.7: Classification results for Strings with defective insulator discs using WPD based features.

Number of healthy insulators in string	Class1	Class 2	Class 3	Overall Rate
1	93	93	96	95
2	94	95	92	96
3	95	92	95	97

result with less than 3% error is obtained, with a 100% recognition rate for class 2 and class 3. These classification steps were repeated for a total of 10 times in order to ascertain a high degree of consistent classification performance. Tables 5.6 and 5.7 tabulate the results corresponding to single discs and defective discs incorporated in strings.

Chapter 6

Conclusions and Future Work

6.1 Summary and Conclusions

The primary objective of the research presented in this thesis was to evaluate the feasibility of detecting defects in ceramic insulators based on the RF signatures that are radiated by PD activity within the insulators. An additional goal was an exploration of the classification of defect types based on the features extracted from the RF signatures. To this end, a number of experiments were conducted in order to assess defective insulator samples: both individual insulators and a string of insulators comprised of a varied number of discs. Based on the results of this work, the following conclusions can be drawn:

1. Each type of defect considered was shown to produce a unique RF signature that can be acquired on a pulse-by-pulse basis using a high-bandwidth oscilloscope. The RF signatures can be identified by unique FFTs as well as by local time-varying characteristics.

2. The PD level (apparent charge value) detectable through the RF technique was demonstrated to have a minimum threshold below which the RF signal cannot be detected by the measuring equipment.

3. Both FFT-based and wavelet-based features can be extracted. The controlled experiments conducted for this study established that wavelet-based features yield a high recognition rate.

4. Trained artificial intelligence (AI) algorithms were shown to be effective for the

classification of each specific type of defect, with a high degree of accuracy: more than 90%.

5. Through repetitive measurements, it was shown that the RF antenna can be up to 2 m from the test sample without compromising the strength of the RF signal detected by the measuring equipment. The distance of the antenna from the insulator string is a critical parameter from the point of view of the personal safety of the line men because every voltage level has a corresponding minimum approach distance.

6. Varying the position of the insulator disc within the string has little or no effect on the level of classification performance.

6.2 Future Work

This work can be extended to address a number of distinct challenges. This section highlights some of the most important.

6.2.1 PD Localisation

In this preliminary work, no consideration was given to the location of the PD within the string. Because this element is important, this work should be extended to include an investigation of the factors related to PD location. Concepts such as the time-of-arrival method could be applied as a means of calculating the distance of the PD source using an array of antennas that feed the different channels of the oscilloscope.

6.2.2 Field Application

All of the experiments related to the research presented in this thesis were carried out in a shielded laboratory environment, which does not include the many sources of interference and noise that are present in a field environment. Testing in the field may therefore provide insights with respect to those sources of noise and their effect on the strength of the RF signal detected by the measuring equipment. An exhaustive library of the RF signals and their correlation with the defects most frequently encountered in the field is envisioned. This library might be valuable for training the AI algorithms

so that when unobservable data are input, the algorithm can classify them according to the defects included in the training.

6.2.3 Relationship between the RF Signal Voltage and the PD Levels Measured Using IEC 60270

Unlike the widely accepted traditional apparent charge measurement technique standardized in IEC 60270, the RF technique is not well-established for measuring PD. For the RF technique to gain wider acceptance, the correlation between RF signals and PD signals measured using the IEC 60270 standard must be determined. The primary goal of such a study would be to establish rules related to the interpretation of RF signals in terms of IEC measurements.

6.2.4 Evaluation of Punctured Insulators

Punctured insulators constitute a major problem for utilities, and their presence represents a possible safety hazard for the line personnel who perform the testing and maintenance tasks. Although this study examined three defect conditions commonly encountered in the field, punctured insulators were not evaluated. Future investigation of the identification of punctured insulators based on the proposed technique would be valuable. For this purpose, field-punctured insulator samples could be obtained through industrial support and tested both individually and in strings.

6.2.5 Automated Vehicle-Mounted System for PD Detection and Classication

The ultimate goal of insulator-testing enhancements should be the development of a prototype system mounted on the top of a vehicle so that RF pulses could be acquired and fed into the trained algorithms. Such a method would enable insulator defects to be detected without the need for permanent hardware to be installed on each transmission line pole. This technique could be extended to include PD localization for testing multiple strings of insulators on transmission line towers. Such a system would necessitate the use of an antenna array comprised of four antennas to capture four signals so that time-difference-of-arrival values could be calculated from the individual RF signatures. The time difference could be further utilized as

a means of computing the distance to the PD-emitting source, and hence, to the defective sample.

List of publications in refereed conference proceedings.

1. S. Anjum , S Jayaram, A. El-Hag and Ali Naderian. " Condition Monitoring system for the detection of defects in ceramic insulators based on their radio frequency (RF) signatures.", the International Conference on Condition Monitroing and Diagnosis 2014 (CMD2014), Jeju Island, Korea, September 21-25, 2014.

2. S. Anjum , S Jayaram, A. El-Hag and Ali Naderian." Classification of Defects in Ceramic Insulators using Partial Discharge Signatures Extracted from Radio Frequency (RF) Signal", IEEE Conference on Electrical Insulators and Dielectric Phenomena (CEIDP2014), Des Moines, IA, USA, October 19-22, 2014.

References

[1] R. Brown and B. Humphrey, "Asset management for transmission and distribution," *Power and Energy Magazine,IEEE*, vol. 3, no. 3, pp. 39–45, 2005.

[2] E. Power-Lines, "IEEE guide for maintenance methods on energized power lines,"

[3] "Transmission Assets And Sustaining Investment Overview," *Hydro One Exhibit C1 Tab 2 Schedule 2*, 2012.

[4] http://www.altalink.ca/valueoftransmission/aes-overview.cfm. Accessed: 2014-09-13.

[5] http://en.wikipedia.org/wiki/Electricpowertransmission. Accessed: 2014-09-13.

[6] S.-H. Kim, E. A. Cherney, R. Hackam, and K. G. Rutherford, "Chemical changes at the surface of RTV silicone rubber coatings on insulators during dry-band arcing," *IEEE Transactions on Dielectrics and Electrical Insulation*, vol. 1, no. 1, pp. 106–123, 1994.

[7] R. S. Gorur, E. A. Cherney, and J. T. Burnham, *Outdoor insulators*. Ravi S. Gorur, 1999.

[8] R. Gorur, E. Cherney, R. Hackam, and T. Orbeck, "The electrical performance of polymeric insulating materials under accelerated aging in a fog chamber," *IEEE Transactions on Power Delivery*, vol. 3, no. 3, pp. 1157–1164, 1988.

[9] R. Hackam, "Outdoor HV composite polymeric insulators," *IEEE Transactions on Dielectrics and Electrical Insulation,*, vol. 6, no. 5, pp. 557–585, 1999.

[10] B. Mills, *Porcelain insulators and how they grew*. Brent Mills, 1970.

[11] E. Cherney, "Electromechanical integrity of suspension insulators," *Ontario Hydro Research Review*, no. 5, pp. 19–23, 1982.

[12] E. Cherney, A. Baker, J. Kuffel, Z. Lodi, A. Phillips, D. Powell, and G. Stewart, "Evaluation of and Replacement Strategies for Aged High Voltage Porcelain Suspension-Type Insulators," 2014.

[13] E. Cherney and R. Hooton, "Cement growth failure mechanism in porcelain suspension insulators," *IEEE Transactions on Power Delivery*, vol. 2, no. 1, pp. 249–255, 1987.

[14] A. Rawat and R. Gorur, "Microstructure based evaluation of field aged and new porcelain suspension insulators," *IEEE Transactions on Dielectrics and Electrical Insulation*, vol. 16, no. 1, pp. 107–115, 2009.

[15] K. Morita, T. Imakoma, M. Nishikawa, and H. Nozaki, "Steep impulse voltage characteristics of suspension insulators," *Electrical engineering in Japan*, vol. 115, no. 2, pp. 21–31, 1995.

[16] E. Zobel, "Insulators lose strength with age," *Elect. World*, pp. 40–42, 1962.

[17] A. Mishra, R. Gorur, and S. Venkataraman, "Evaluation of porcelain and toughened glass suspension insulators removed from service," *IEEE Transactions on Dielectrics and Electrical Insulation*, vol. 15, no. 2, pp. 467–475, 2008.

[18] G. Vaillancourt, J. Bellerive, M. St-Jean, and C. Jean, "New live line tester for porcelain suspension insulators on high-voltage power lines," *IEEE Transactions on Power Delivery*, vol. 9, no. 1, pp. 208–219, 1994.

[19] M. Ostendorp, "Assessing the integrity and remaining service life of vintage high voltage ceramic insulators," in *IEEE 10th International Conference on Transmission and Distribution Construction, Operation and Live-Line Maintenance, 2003. 2003 IEEE ESMO.2003*, pp. 169–175, IEEE, 2003.

[20] E. Subcommittee, "Minimum number of good (healthy) porcelain or glass insulator units in a string for live work," *Power Engineering Review, IEEE*, vol. 22, no. 5, pp. 71–71, 2002.

[21] C. Nyamupangedengu, L. Luhlanga, and T. Letlape, "Acoustic and hf detection of defects on porcelain pin insulators," in *Power Engineering Society Conference and Exposition in Africa, 2007. PowerAfrica'07.*, pp. 1–5, IEEE, 2007.

[22] H. Ha, S. Han, and J. Lee, "Fault detection on transmission lines using a microphone array and an infrared thermal imaging camera," *IEEE Transactions on Instrumentation and Measurement*, vol. 61, no. 1, pp. 267–275, 2012.

[23] E. Cherney and D. Amm, "Development and application of a hot-line suspension insulator tester," *IEEE Transactions on Power Apparatus and Systems*, no. 4, pp. 1525–1528, 1981.

[24] J. C. Pohlman and C. R. Davis, "Cracked insulators create hazardous working conditions during restoration after extreme ice storm," in *Seventh International Conference on Transmission and Distribution Construction and Live Line Maintenance, 1995. ESMO-95 Proceedings.*, pp. 143–149, IEEE, 1995.

[25] Y. Cheng, C. Li, and B. Liu, "The sensitivity of electric field method on detecting faulty porcelain insulators," in *8th International Conference on Properties and applications of Dielectric Materials, 2006.*, pp. 615–618, IEEE, 2006.

[26] D. Auckland, A. McGrail, C. Smith, B. Varlow, J. Zhao, and D. Zhu, "Application of ultrasound to the inspection of insulation," in *IEE Proceedings on Science, Measurement and Technology.*, vol. 143, pp. 177–181, IET, 1996.

[27] I. E. Commission *et al.*, "IEC 60270 Standard," *High-voltage test techniques–Partial discharge measurements*, 2000.

[28] J. Kuffel, E. Kuffel, and W. S. Zaengl, *High voltage engineering fundamentals*. Newnes, 2000.

[29] A. Haddad and D. F. Warne, *Advances in high voltage engineering*, vol. 40. IET, 2004.

[30] P. J. Moore, I. E. Portugues, and I. A. Glover, "Radiometric location of partial discharge sources on energized high-voltage plant," *IEEE Transactions on Power Delivery*, vol. 20, no. 3, pp. 2264–2272, 2005.

[31] A. Cavallini, G. Montanari, A. Contin, and F. Pulletti, "A new approach to the diagnosis of solid insulation systems based on pd signal inference," *IEEE Electrical Insulation Magazine*, vol. 19, no. 2, pp. 23–30, 2003.

[32] N. De Kock, B. Coric, and R. Pietsch, "UHF PD detection in gas-insulated switchgear-suitability and sensitivity of the UHF method in comparison with the IEC 270 method," *IEEE Electrical Insulation Magazine*, vol. 12, no. 6, pp. 20–26, 1996.

[33] J. Pearson, B. Hampton, and A. Sellars, "A continuous uhf monitor for gas-insulated substations," *IEEE Transactions on Electrical Insulation*, vol. 26, no. 3, pp. 469–478, 1991.

[34] A. Petit, "Field experience of partial discharge monitoring with the UHF method," *Collection de notes internes-direction des etudes et recherches electricite de France materiel electrique transport et distribution de energie*, 1996.

[35] R. Kurrer, K. Klunzinger, K. Feser, N. De Kock, and D. Sologuren, "Sensitivity of the uhf-method for defects in gis with regard to on-line partial discharge detection," in *Conference Record of the 1996 IEEE International Symposium on Electrical Insulation, 1996.*, vol. 1, pp. 95–98, IEEE, 1996.

[36] B. Hampton, "The spectra of corona discharges in air and sf6," in *GD 85: Proc. 8th Int. Conf. Gas Discharges and their Applications*, pp. 209–11, 1985.

[37] T. Ju, X. Zhongrong, Z. Xiaoxing, and S. Caixin, "GIS partial discharge quantitative measurements using UHF microstrip antenna sensors," in *Annual Report-Conference on Electrical Insulation and Dielectric Phenomena, 2007. CEIDP 2007.*, pp. 116–119, IEEE, 2007.

[38] P. J. Orr, A. J. Reid, and M. D. Judd, "Sensor response characteristics for UHF location of PD sources," in *Condition Monitoring and Diagnosis, 2008. CMD 2008. International Conference on*, pp. 1119–1122, IEEE, 2008.

[39] T. Pinpart and M. Judd, "Experimental comparison of UHF sensor types for

PD location applications," in *Electrical Insulation Conference, 2009. EIC 2009. IEEE*, pp. 26–30, IEEE, 2009.

[40] T. Li, X. Wang, C. Zheng, D. Liu, and M. Rong, "Investigation on the placement effect of uhf sensor and propagation characteristics of PD-induced electromagnetic wave in GIS based on FDTD method," *IEEE Transactions on Dielectrics and Electrical Insulation*, vol. 21, no. 3, pp. 1015–1025, 2014.

[41] S. Kaneko, S. Okabe, M. Yoshimura, H. Muto, C. Nishida, and M. Kamei, "Detecting characteristics of various type antennas on partial discharge electromagnetic wave radiating through insulating spacer in gas insulated switchgear," *IEEE Transactions on Dielectrics and Electrical Insulation*, vol. 16, no. 5, pp. 1462–1472, 2009.

[42] W. Putro, K. Nishigouci, U. Khayam, M. Kozako, M. Hikita, K. Urano, C. Min, *et al.*, "PD pattern of various defects measured by uhf external sensor on 66 kV GIS model," in *2012 International Conference on Condition Monitoring and Diagnosis (CMD)*, pp. 954–957, IEEE, 2012.

[43] S. Okabe, T. Yamagiwa, and H. Okubo, "Detection of harmful metallic particles inside gas insulated switchgear using UHF sensor," *IEEE Transactions on Dielectrics and Electrical Insulation*, vol. 15, no. 3, pp. 701–709, 2008.

[44] S. Tenbohlen, D. Denissov, S. Hoek, and S. Markalous, "Partial discharge measurement in the ultra high frequency (UHF) range," *IEEE Transactions on Dielectrics and Electrical Insulation*, vol. 15, no. 6, pp. 1544–1552, 2008.

[45] H. Imagawa, K. Emoto, H. Murase, H. Koyama, R. Tsuge, S. Maruyama, and T. Sakakibara, "PD signal propagation characteristics in GIS and its location system by frequency components comparison," *IEEE Transactions on Power Delivery*, vol. 16, no. 4, pp. 564–570, 2001.

[46] R. Bell, C. Charlson, S. P. Halliday, T. Irwin, J. Lopez-Roldan, and J. Nixon, "High-voltage onsite commissioning tests for gas-insulated substations using UHF partial discharge detection," *IEEE Transactions on Power Delivery*, vol. 18, no. 4, pp. 1187–1191, 2003.

[47] M. Judd, O. Farish, J. Pearson, and B. Hampton, "Dielectric windows for UHF partial discharge detection," *IEEE Transactions on Dielectrics and Electrical Insulation*, vol. 8, no. 6, pp. 953–958, 2001.

[48] M. Hikita, S. Ohtsuka, T. Teshima, S. Okabe, and S. Kaneko, "Electromagnetic (EM) wave characteristics in GIS and measuring the EM wave leakage at the spacer aperture for partial discharge diagnosis," *IEEE Transactions on Dielectrics and Electrical Insulation*, vol. 14, no. 2, pp. 453–460, 2007.

[49] M. Hikita, S. Ohtsuka, T. Teshima, S. Okabe, and S. Kaneko, "Examination of electromagnetic mode propagation characteristics in straight and L-section GIS model using FD-TD analysis," *IEEE Transactions on Dielectrics and Electrical Insulation*, vol. 14, no. 6, pp. 1477–1483, 2007.

[50] T. Hoshino, S. Maruyama, and T. Sakakibara, "Simulation of propagating electromagnetic wave due to partial discharge in GIS using FDTD," *IEEE Transactions on Power Delivery*, vol. 24, no. 1, pp. 153–159, 2009.

[51] M. D. Judd, L. Yang, and I. B. Hunter, "Partial discharge monitoring of power transformers using UHF sensors. Part I: sensors and signal interpretation," *IEEE Electrical Insulation Magazine*, vol. 21, no. 2, pp. 5–14, 2005.

[52] M. D. Judd, L. Yang, C. J. Bennoch, and I. B. Hunter, "UHF diagnostic monitoring techniques for power transformers," in *EPRI Substation Equipment Diagnostics Conference, New Orleans*, 2004.

[53] B. Stewart, D. Hepburn, I. Kemp, A. Nesbitt, and J. Watson, "Detection and characterisation of partial discharge activity on outdoor high voltage insulating structures by RF antenna measurement techniques," in *High Voltage Engineering, 1999. Eleventh International Symposium on (Conf. Publ. No. 467)*, vol. 5, pp. 188–191, IET, 1999.

[54] I. Y. Shurrab, A. H. El-Hag, K. Assaleh, R. A. Ghunem, and S. Jayaram, "RF-based monitoring and classification of partial discharge on wet silicone rubber surface," *IEEE Transactions on Dielectrics and Electrical Insulation*, vol. 20, no. 6, pp. 2188–2194, 2013.

[55] K. L. Wong, "Application of very-high-frequency (VHF) method to ceramic insulators," *IEEE Transactions on Dielectrics and Electrical Insulation*, vol. 11, no. 6, pp. 1057–1064, 2004.

[56] P. Moore, I. Portugues, and I. Glover, "Remote diagnosis of overhead line insulation defects," in *IEEE Power Engineering Society General Meeting, 2004.*, pp. 1831–1835, IEEE, 2004.

[57] N. K. Nicolova, "Lecture 18: Horn antennas." McMaster University Lecture, 2010.

[58] C. A. Balanis, *Antenna theory: analysis and design*. John Wiley & Sons, 2012.

[59] P. Wang, A. Cavallini, G. C. Montanari, and G. Wu, "Effect of rise time on PD pulse features under repetitive square wave voltages," *IEEE Transactions on Dielectrics and Electrical Insulation*, vol. 20, no. 1, pp. 245–254, 2013.

[60] N. Sahoo, M. Salama, and R. Bartnikas, "Trends in partial discharge pattern classification: a survey," *IEEE Transactions on Dielectrics and Electrical Insulation*, vol. 12, no. 2, pp. 248–264, 2005.

[61] S. Wenrong, L. Junhao, Y. Peng, and L. Yanming, "Digital detection, grouping and classification of partial discharge signals at DC voltage," *IEEE Transactions on Dielectrics and Electrical Insulation*, vol. 15, no. 6, pp. 1663–1674, 2008.

[62] M. Bramer, *Principles of data mining*. Springer, 2013.

[63] R. A. Gopinath and H. ta Guo, "Introduction to wavelets and wavelet transforms: a primer," 1997.

[64] D. L. Donoho, "De-noising by soft-thresholding," *IEEE Transactions on Information Theory*, vol. 41, no. 3, pp. 613–627, 1995.

[65] S. Mallat and S. Zhong, "Characterization of signals from multiscale edges," *IEEE Transactions on pattern analysis and machine intelligence*, vol. 14, no. 7, pp. 710–732, 1992.

[66] D. L. Donoho, Johnstone, and I. M, "Ideal denoising in an orthonormal basis chosen from a library of bases," *Comptes rendus de l'Académie des sciences. Série I, Mathématique*, vol. 319, no. 12, pp. 1317–1322, 1994.

[67] N. Verma and A. Verma, "Performance analysis of wavelet thresholding methods in denoising of audio signals of some indian musical instruments," *International Journal of Engineering Science and Technology*, vol. 4, no. 5, pp. 2040–2045, 2012.